AD NUMBER

AD486993

NEW LIMITATION CHANGE

TO

Approved for public release, distribution unlimited

FROM

Distribution authorized to U.S. Gov't. agencies and their contractors; Administrative/Operational Use; 1 May 1966. Other requests shall be referred to U.S. Army Engineer Research and Development Labs., Fort Belvoir, VA.

AUTHORITY

COE ltr, 13 Jul 1971

NUCLEAR ELECTROMAGNETIC PULSE SIMULATION STUDIES IN SUPPORT OF THE NIKE-X ELECTRICAL POWER SYSTEM PROGRAM

FINAL TECHNICAL REPORT (REVISED)

Period Covered: 1 November 1964 - 31 October 1965

1 May 1966

Prepared By:

Ronald J. Bostak
A. Russell Bemis

U. S. Army Engineer Research and Development Laboratories
Fort Belvoir, Virginia

This research has been sponsored by the Office, Chief of Engineers in support of the Nike-X Electrical Power System Research and Development Program.

All distribution of this report is controlled. Qualified DDC users should request through Office, Chief of Engineers, DA, ATTN: ENGMC-ED, Washington, D. C. 20315.

SUMMARY

This report presents the results that have been achieved at USAERDL during the period November 1964 through October 1965 in nuclear EMP simulation studies and experimentation in support of the Nike-X electrical power system research and development program. These studies and experiments can be classified as EMP vulnerability testing of existing systems, basic EMP energy coupling experimentation, and EMP simulation or experimental facility design which includes electromagnetic field measurement instrumentation design and development. The experimental results in this report are documented as companion data to theoretical results published in a previous report.

TABLE OF CONTENTS

TABLE OF CONTENTS (CONT)

LIST OF ILLUSTRATIONS

LIST OF ILLUSTRATIONS (CONT)

1. INTRODUCTION

Due to increased concern over EMP effects, theoretical and experimental efforts to understand the manner in which EMP energy couples into systems and means for hardening systems against EMP effects have been accelerated in the last few years. Theoretical prediction of military system operation in an EMP environment bogs down in the complexities of real systems. The most promising approach to develop a quantitative understanding of EMP energy coupling, system EMP vulnerability and the effectiveness of EMP hardening measures is through coordinated programs of theoretical studies and experimental studies using EMP simulation techniques. Experimental data must be utilized to:

a. Determine the coupling between given electromagnetic environments and items under study.

b. Determine vulnerabilities of the items to this environment.

c. Design protective techniques for the items.

d. Test the effectiveness of the protective techniques developed.

The experimental data necessary to accomplish the above objectives can be obtained through different experimental techniques; however, no one technique appears to be adequate to supply all the

necessary data. For this reason, systematic experimental programs tailored to the specific problem are necessary. These programs fall into the following two related categories at present: vulnerability testing of existing systems and basic energy coupling experimentation to obtain design data for systems in the planning or design phase which are not existing at present. Each category complements the other for experimental data on existing systems can be used to influence the design of newer systems and basic energy coupling data can be used to assist in the understanding of vulnerabilities of existing systems leading to corrections where necessary.

Two fundamental experimental techniques can be and are presently being employed in both the above categories. These are high peak amplitude pulsed field experimentation and low amplitude sinusoidal frequency response experimentation. Although treated as separate experimental techniques, it is important to note that there is much in common between the two. When systems or mechanisms under investigation can be described as linear, pulse experimentation and frequency response experimentation may be correlated through the Fourier transform pair for causal functions

$$f(\omega) = \frac{1}{2\pi} \int_{-\infty}^{+\infty} f(t)\, e^{-j\omega t}\, dt \qquad (1)$$

$$f(t) = \int_{-\infty}^{+\infty} f(\omega)\, e^{j\omega t}\, d\omega$$

It would appear advisable in such cases to choose the expedient

experimental technique or, when possible, to use both techniques to establish the linearity of the system or mechanism. This philosophy has been adopted for the shielding investigations described in another ERDL report, and conducted in the EMP Experimental Facility at USAERDL.

In those cases where linearity of response cannot be established, only high peak amplitude pulse field experimentation serves as a valid experimental technique. This field must be indicative of the actual EMP environment of interest to provide meaningful data. Inherently, the high peak amplitude pulse field experimental technique is the more difficult to conduct of the two techniques. Unfortunately, common construction materials such as steel are non-linear and digital logic circuits by design are non-linear; the response of such items can be critical determinants of military system vulnerability to the EMP.

The determination of the susceptibility of a military system to the EMP is in reality a system problem since major uncertainties are involved in combining component response to obtain a system response. At best, only GO, NO-GO responses are predictable in very simple systems using a summation of separately determined component responses; the latter being orders of magnitude more predictable than the former. Experiments conducted on existing systems to date and described in Chapter 2, In Situ Electromagnetic Field Tests at the Nevada Test Site, have used the

system concept to as large an extent as possible. To create a full amplitude electromagnetic environment over a large military system such as Nike-X, however, would require drive systems of extremely high energy levels. In such cases selection of the largest separable subsystem is the only alternative approach. Experiments to be conducted in the EMP Simulation Facility will follow the above philosophy.

2. IN SITU ELECTROMAGNETIC FIELD TESTS AT THE NEVADA TEST SITE

When analyzing real systems to determine the energy coupling from an incident electromagnetic field, it becomes rather apparent that in many cases the non-calculable non-idealizations of construction are overwhelmingly the dictating response mechanism. For this reason, it will be necessary to real-life test military systems for EMP vulnerability. Similarly, it appears reasonable to test real-life experimental configurations on an in situ basis. Results reported[1] on experimental verification of nuclear weapons effects test data obtained during shot Small Boy are extensions of this philosophy. A description of this experiment is found herein. Results of these tests indicate more conclusively that system test concepts are extremely valuable.

---

[1] Superscripts refer to list of references located at end of report.

2.1 Objective

To increase the understanding of the EMP induced current distributions observed on the cable array during the Small Boy nuclear weapons effects test, Stanford Research Institute (SRI) conducted a series of non-nuclear tests using an electrically short antenna source, field measuring equipment, and cable current monitoring instrumentation. Calculated and measured fields for low frequency antenna systems had shown that continuous wave (CW) and p d transmitters could be employed to further define cable coupling phenomena. A description of the system used by SRI, the test results, and the comparisons with theory are described in an Air Force Weapons Laboratory report[2]. This work was jointly sponsored by the Air Force Weapons Laboratory (AFWL) and USAERDL.

2.2 Test Description

The 100 foot high monopole antenna shown in Figure 1 was installed in Area 5 at the Nevada Test Site and was driven with a CW transmitter and with a pulse transmitter. Measurements of the electromagnetic field were made over an area containing the various buried cables and bunkers installed for Shot Small Boy. Electric and magnetic field magnitude and phase were measured for the CW fields and the time signatures were recorded on oscilloscope-camera units for the pulsed fields. Similar measurements were made

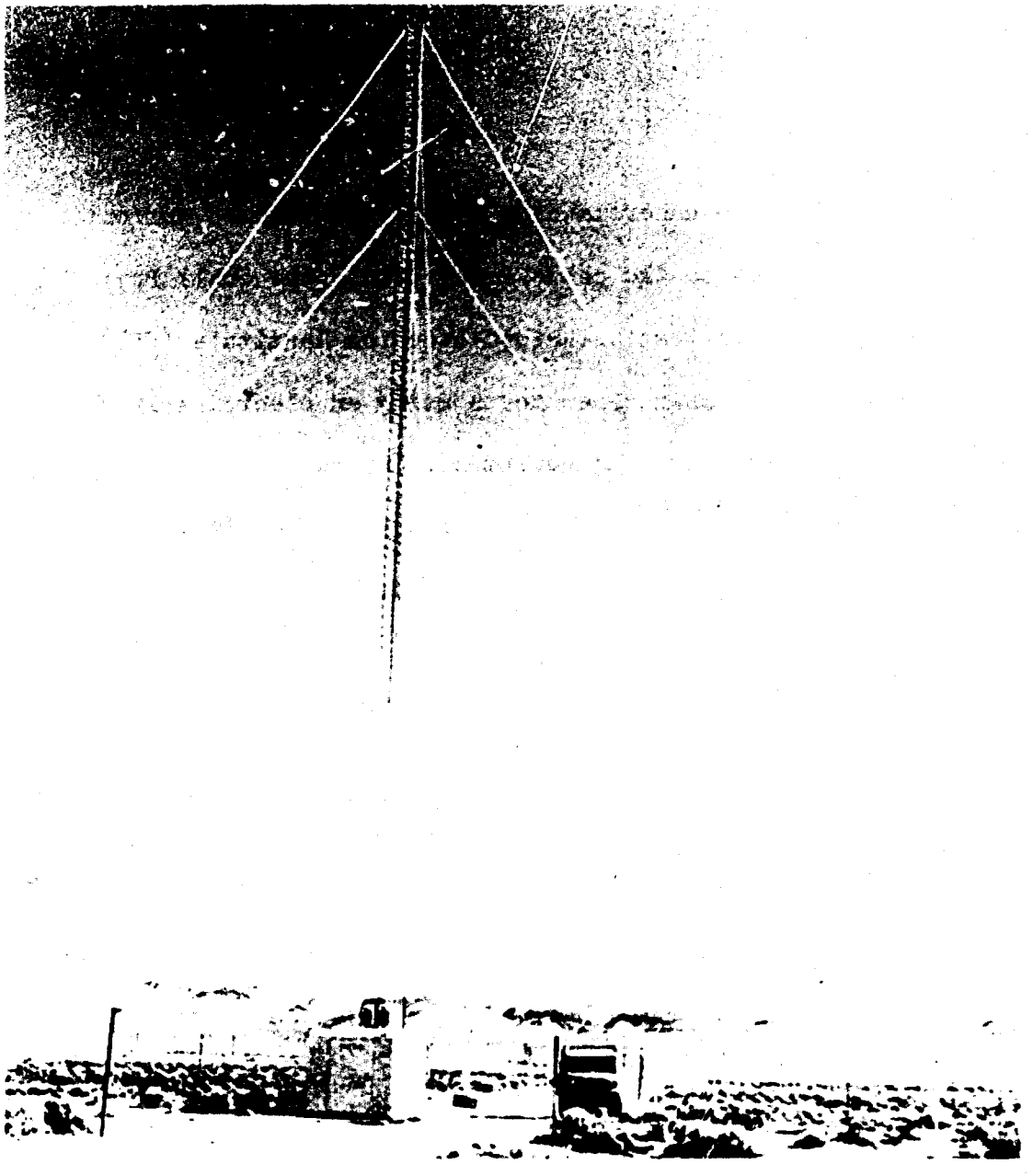

FIGURE 1. ONE HUNDRED FOOT MONOPOLE ANTENNA

of the currents induced into cables located in the area. Since there were many non-idealized boundaries in the area, including the presence of the earth media, free-space relationships could not be

used to relate the electric and magnetic fields.

2.3 Transmitter

In the CW measurements, eleven fixed frequencies were transmitted from 0.5 kilocycles to 510 kilocycles. A wideband power amplifier drove the antenna which was capacitive at these frequencies through a resonating coil in series. Tuning of the antenna was accomplished by replacement of the series coil for the various frequencies. A vacuum tuning capacitor was used for trimming the system. Antenna voltage was monitored using a capacitive probe located at its base.

The pulse generator for the transmitter consisted of two capacitor banks that were charged in parallel and discharged in series. A 120 kilovolt rectifier power supply was used to charge the capacitors through two 20 megohm resistors. Discharge of the circuits occurs when one of the gaps, set to break down at 100 kilovolts, fires and applies the total voltage across the other gap. When the second gap fires, the capacitors appear as series connected through the spark gaps to the antenna and a pulse shaping circuit.

2.4 Receivers

The receiving equipment consisted of portable battery powered preamplifiers, tuned receivers, and calibration oscillators. Electric field measurements were made with a parallel plate antenna with an effective height of 0.16 meters. The two mesh plates were 1.5 meters on a side and were separated by phenolic insulators. Orientation of the antenna was accomplished by a swivel

and gimbal arrangement. The minimum sensitivity of this antenna was 0.1 microvolt per meter at 0.5 kilocycles and 0.004 microvolts per meter at 510 kilocycles. For each fixed frequency, the antenna was tuned and matched to a low-noise, wideband preamplifier.

Magnetic fields were detected with a single turn loop antenna, constructed of 2 inch aluminum pipe in a square shape 1.5 meters on a side. Threshold levels of this antenna were from 10^{-8} ampere turns per meter at 0.5 kilocycles to $3(10)^{-10}$ ampere turns per meter at 510 kilocycles. This antenna was tuned and matched to a sensitive wideband preamplifier to obtain sensitivity. Positioning of the antenna was also accomplished by a gimbal and swivel arrangement as in the plate antenna.

Two phase quadrature synchronous reference signals were used to determine the amplitude and phase of the measured signal. The phase reference was the vertical electric field and two sensitive meters were used to determine the quadrature components of the signal.

Cable current measurements were made with a toroidal pickup coil having a core of Mo-permalloy for the low frequency measurements and a core of ferrite for the high frequency measurements. For the CW cable current measurements, the data were monitored from meters on the receiver units. The pulse measurements were obtained from a self-triggering oscilloscope and transparent polaroid film.

2.5 Conclusions

The measurements obtained provided an electromagnetic map of the area showing the field distortions present. Amplitude measurements were accurate to within 3 percent and phase to within 5 degrees for both the magnetic and electric fields. Cable current measurements on buried cables were correlated with the electromagnetic fields at the earth's surface. The pulse measurements were consistent with the data obtained from the CW tests. In the measurement of complex electromagnetic coupling, there appears to be a definite advantage in using pulse testing techniques because peaks and nulls in responses show up directly. However, the measurement accuracy in pulse testing cannot approach that of fixed frequency testing because of the wide bandwidth requirement of the former.

3. EMP SIMULATION FACILITY

The EMP Simulation Facility briefly described herein was conceived as a research tool to meet experimental needs of the EMP community, modestly but immediately. It is not the answer to the hopes of those desiring a simulated nuclear detonation environment but is a facility in which those effects which are electromagnetic only can be studied. Inclusion of other effects such as transient radiation may be possible on a modest scale in the future.

3.1 Description

The EMP Simulation Facility is located within the USAERDL North Area, Fort Belvoir, Virginia, as shown in Figure 2.

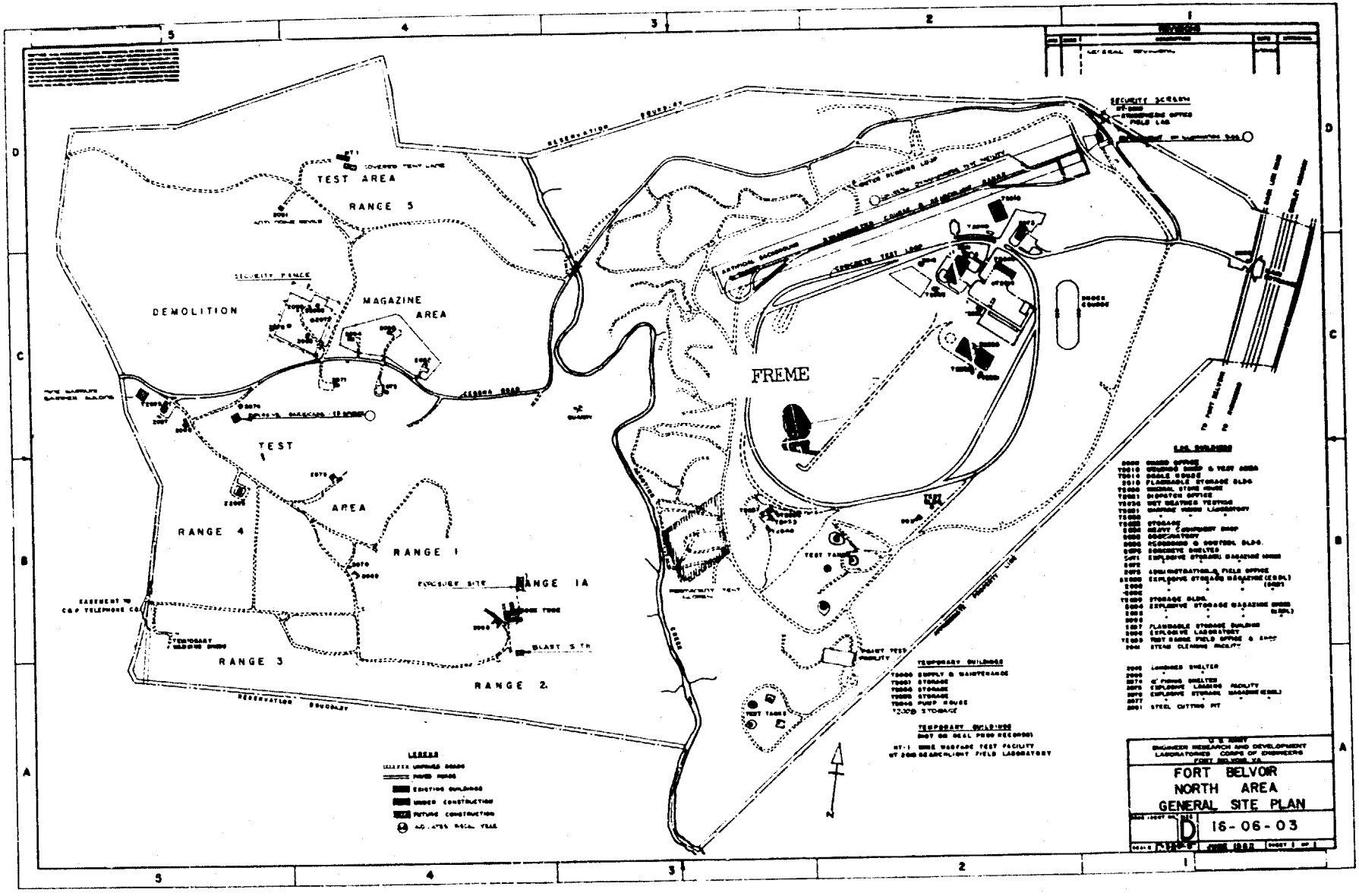

FIGURE 2 FACILITY LOCATION

Surrounding real estate is of lower elevation than the site, allowing for minimum reflection of self generated signals. Figure 3 shows the relative locations of the major items in the facility and the support items which are integral with operation of the facility as an autonomous laboratory. The complete work area is covered with light gravel to permit variation of soil conductivity at any time by scraping, watering, chemical seeding, or combinations of each.

The facility is weather protected over much of its area by a 210 feet diameter hemispherical air supported structure similar to the type commonly used as radome. This structure is relatively transparent to electromagnetic signals in the frequency band of interest provided that no snow or ice is coating the outer surface; measures have been taken to remove such accumulation when they occur.

High volume low velocity blowers automatically maintain a one inch water column pressure inside the structure for external ambient winds below 50 miles per hour and raise and maintain a two inch water column pressure inside the structure for external ambient winds above 50 miles per hour. Structure design is for an external ambient wind of 70 miles per hour over prolonged periods of time.

The air supported structure is attached at its base to a concrete curb which is 16 inches wide and which extends 1 foot above grade and 5 feet below grade. In order for minimum metal to be included in the work area, no horizontal reinforcing steel is used in this curb. Forces on the concrete require, however, that a vertical rebar be provided every two feet around the structure where

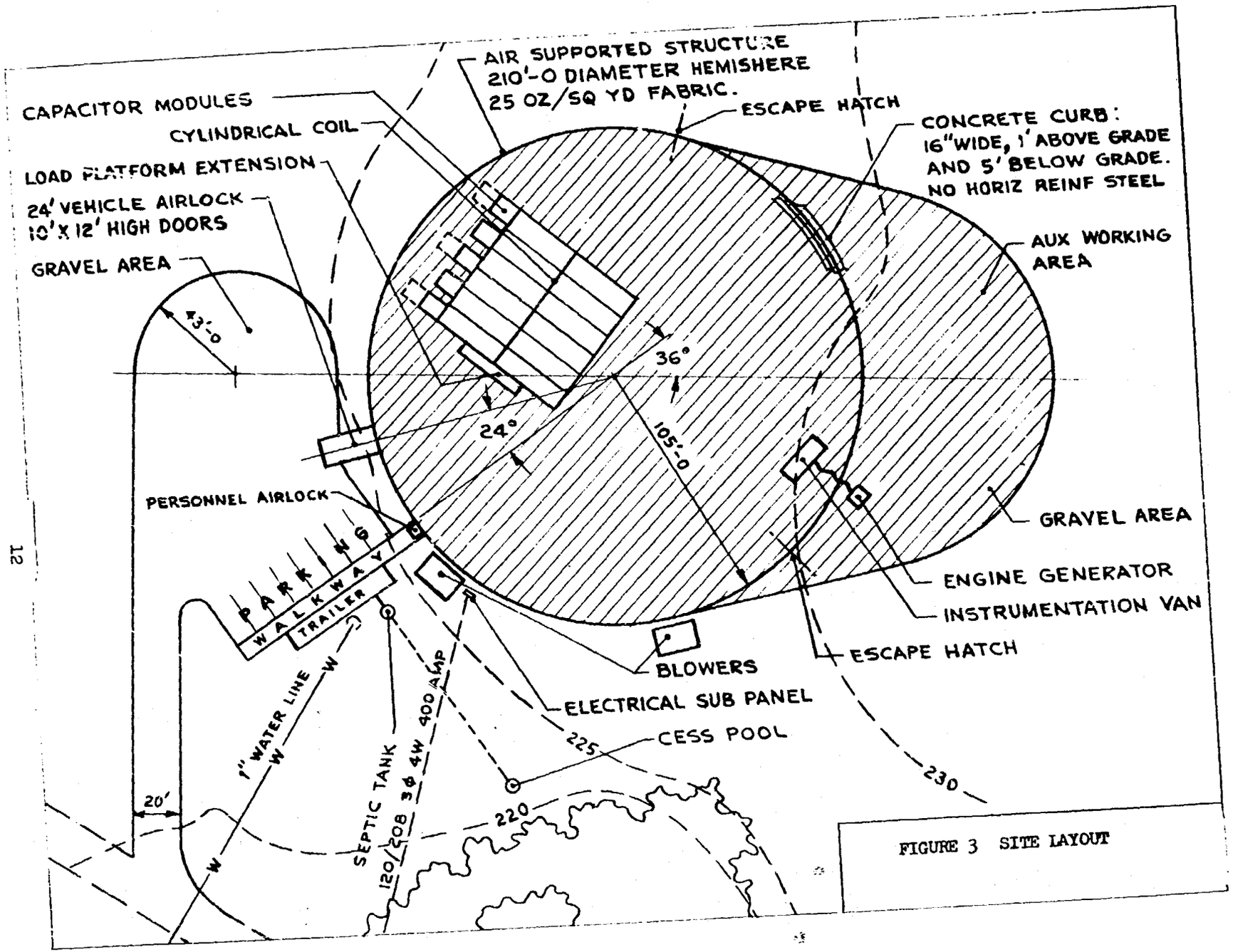

FIGURE 3 SITE LAYOUT

the envelope attaches to the curb.

A large equipment airlock provides entrance to and exit from the air supported structure. It is 24 feet long and has 12 feet high by 10 feet wide doors which are interlocked to prevent air escape. Equipment which is larger than the above airlock can be moved in and out by deflating and opening the structure. However, due to abnormal fabric stresses developed and the large numbers of operating personnel required during this procedure, considerable justification is necessary. A personnel airlock is located near the laboratory trailer. The 10 foot by 50 foot laboratory trailer is available for calibration and fabrication of electronics. Facilities include desk space, lab benches, tools, common electronics laboratory instrumentation, and darkroom facilities. Facility operation is supervised from this location.

The principal electromagnetic field source at the EMP Simulation Facility consists of a conducting cylindrical coil 51 feet in diameter and 60 feet axial length containing a set of thin conducting parallel plates electrically isolated from the conducting cylindrical skin as shown in Figure 4. Horizontal magnetic fields and vertical electric fields are independently created within this coil by utilizing separate driving systems. The magnetic field is essentially uniform and unidirectional within the structure. The uniformity of the electric field depends upon temporary voltage divided guard rings which are spaced between the conducting plates during particular experiments.

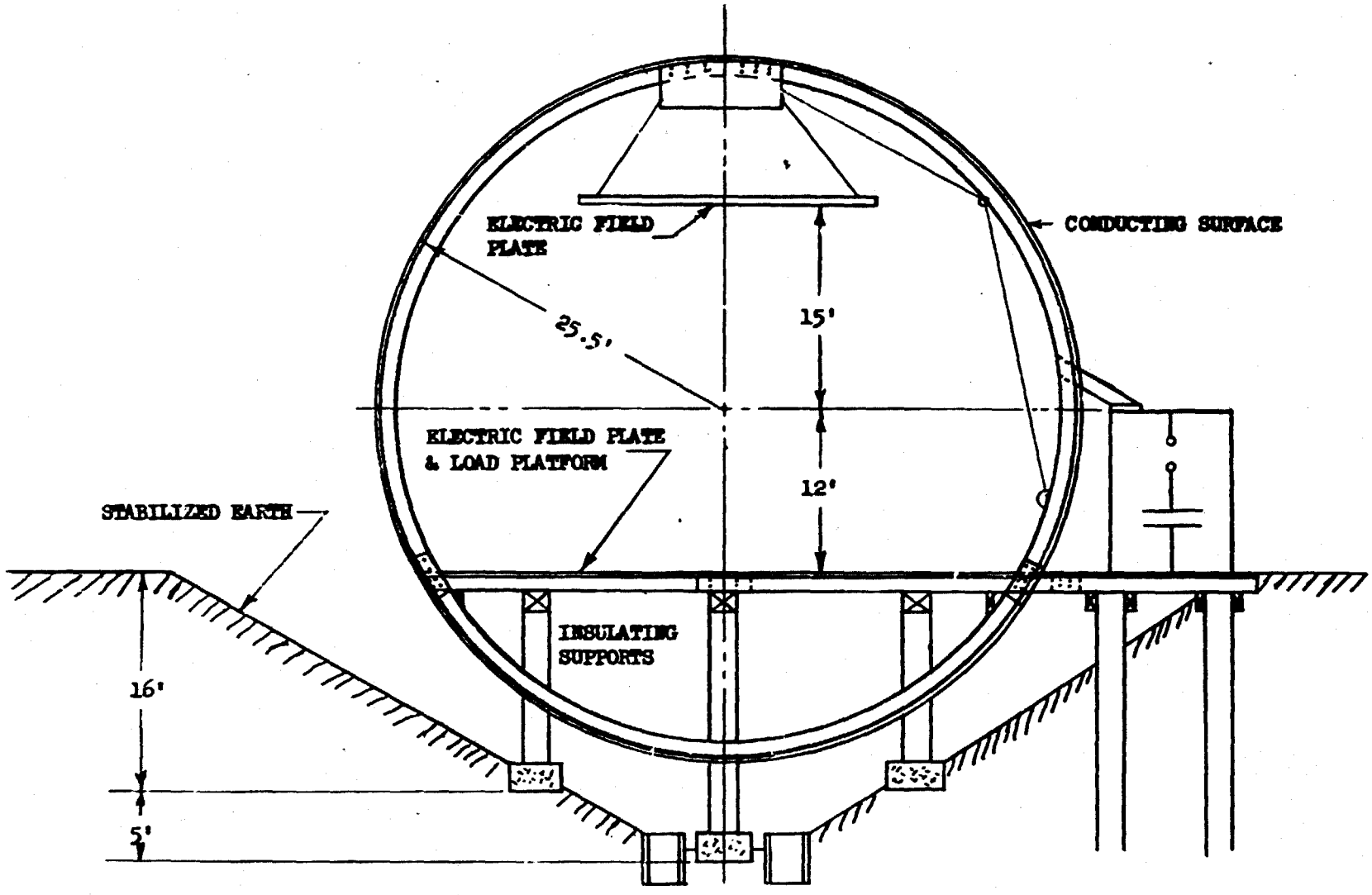

FIGURE 4 CYLINDRICAL COIL

An electrically isolated platform capable of supporting wheeled loads up to 10 tons is located within the coil at ground elevation. The working volume is 60 feet long by 30 feet wide by 27 feet high.

A representative time signature of the electromagnetic fields within the coil is that of a damped sinusoid of 3.4 microsecond risetime, 11.5 microsecond crossover and a 10 percent reversal. The waveform is continuously adjustable in peak amplitude from 20 percent of full value up to a full value of 60 gauss and 100,000 volts per meter. It is adjustable in time characteristics over a wide range of values; however, faster risetimes and shorter crossover times degrade the peak amplitude available. Slower risetimes and longer crossover times are readily adjusted in increments to eight times the values stated. Experiments requiring fields with faster time signatures can be conducted at maximum amplitudes over smaller volumes using other techniques.

Two other field sources will be constructed in the future to create fields over larger volumes. These sources consist of two 30 degree fanned cable systems held approximately 50 feet aloft terminating to ground at points which are segments of circles 100 feet and 250 feet from the pulsed energy source. Fields created within these wedge shaped coils will be of relatively low amplitude but will have risetimes much shorter than those obtainable in the cylindrical coil. The $\vec{E}$ to $\vec{H}$ relationship will be determined by the terminating elements attached to the cables.

The five Marx generators modules have dimensions 8 feet by 10 feet by 10 feet high and are of such design that they may be stacked in series to form a 5 million volt Marx generator. Capacitors are arranged within each module in a staircase configuration for ease of servicing. The structure itself is constructed of fiberglass members with permali and plexaglass coverings. Spark gaps operating in air are used for all switching functions and distributed resistance is of a plug-in type to allow for rapid waveshape modifications. Corona shields are provided at the top of each module.

The cylindrical coil is operated to produce relatively uniform magnetic fields. The pulsed energy source drives the coil with essentially a uniformly distributed current. This is accomplished with five Marx generators in parallel along one side of the coil at equally distributed points. The Marx generators are then triggered within 0.2 microsecond of each other to supply the uniformity of current distribution required. By placing the Marx generators close to the side of the coil, minimum inductive and resistive losses will occur along feeding lines.

The following lumped parameters can be assigned to the complete system assuming a total circuit resistance of the

coil and the capacitor bank of 5.95 ohms:

Current	- 100,000 amperes
Voltage	- 1,000,000 volts
Inductance	- 15 microhenries
Capacitance	- 0.6 microfarad
Resistance	- 5.95 ohms
Risetime	- 3.4 microseconds
Period	- 23 microseconds
Energy	- 300 kilojoules

The electric field plates within the coil are driven by a separate capacitor bank in order to match the waveshape of the magnetic field.

An autonomous and transportable instrumentation system has been developed at USAERDL for the EMP Simulation Facility. The sensors have been designed to extract minimum energy from the field to be measured thereby causing minimum distortion. In all cases this equipment has been experimentally evaluated to determine its susceptibility to high transient electromagnetic fields. No attempt

has been made to develop nuclear weapons effects test hardened instruments except where inherently possible at minimum sacrifice to laboratory standards. More detailed information about this equipment is contained in Chapter 5, Instrumentation Development.

3.2 Schedule

The EMP Simulation Facility is presently under construction at USAERDL. Final construction should be completed by May 1966 and check out and acceptance testing will begin immediately. USAERDL will conduct a series of controlled experiments to establish the electromagnetic characteristics of the system and to obtain preliminary test data. The Facility will be available for use by other agencies by late Spring 1966. Operating personnel will be supplied by USAERDL for the Facility itself. Operation of equipment or items under test will be the responsibility of the using agency.

4. EMP EXPERIMENTAL FACILITY

The EMP Experimental Facility[3] located at USAERDL within Building 326 is operational on a day-to-day basis for conducting pulsed field experiments in support of in-house theoretical programs and as a design and development tool for the EMP Simulation Facility under construction. The principal component of the Experimental Facility is a pulsed energy source which consists of four large storage capacitors, a discharge tank, a trigger gap assembly and appropriate controls. A simplified schematic of the pulsed energy source is shown in Figure 5. The capacitors are connected in parallel between the distribution plate and the discharge tank. A

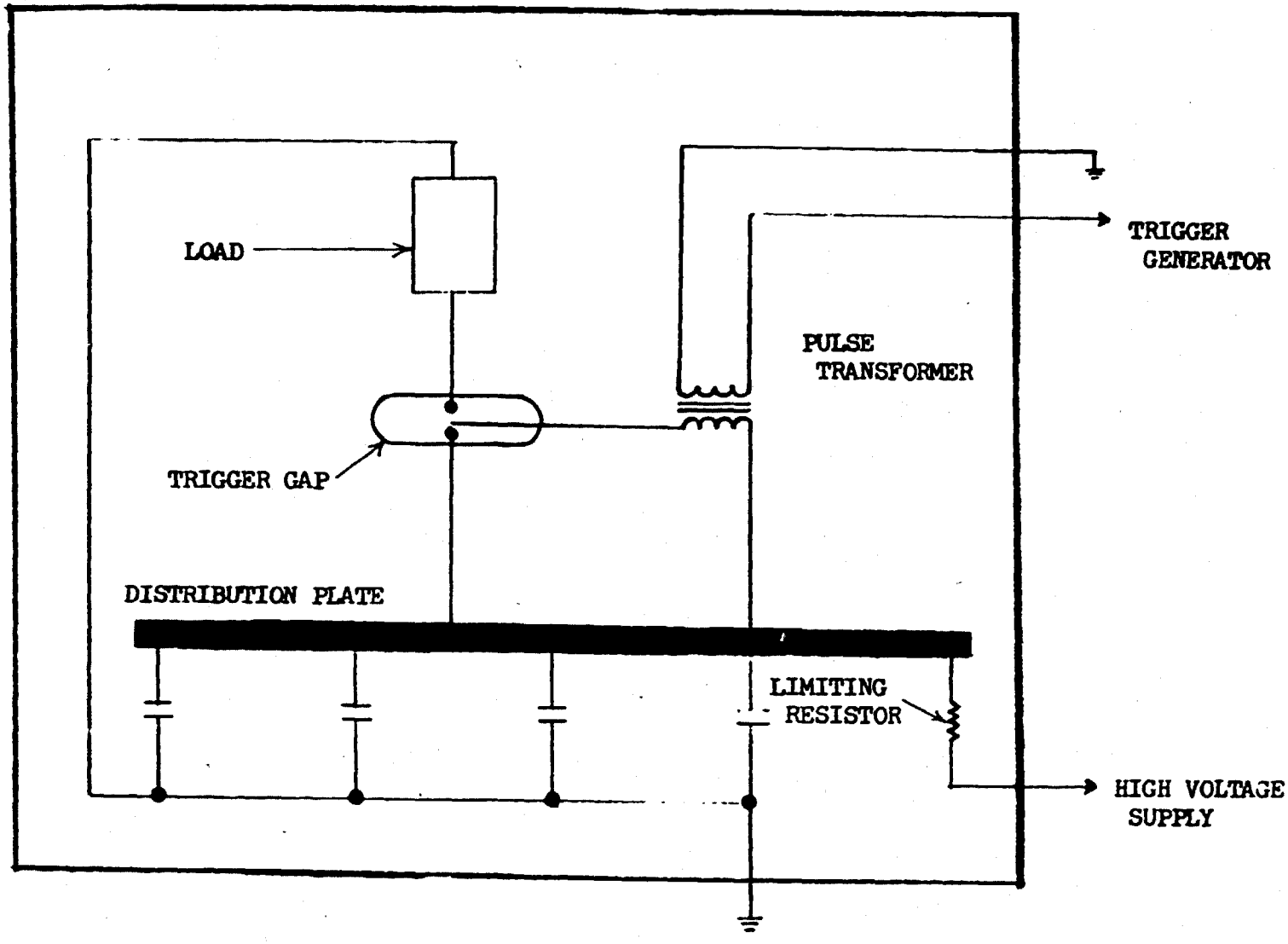

FIGURE 5 SIMPLIFIED SCHEMATIC OF PULSED-ENERGY SOURCE

high voltage power supply is used to charge the capacitors. Stored energy is switched into the load by a trigger gap assembly. This gap is used to dump the capacitor charge through an appropriate load. Associated equipment necessary for the control and safe operation of the unit includes an oil-handling system, a high voltage power supply, a high voltage bleed-off tank, a trigger gap pressure control system, control and monitoring equipment, and support equipment. This equipment was originally designed by Edgerton, Germeshausen & Grier, Inc., Boston, Massachusetts, but has been appreciably modified by USAERDL.

The capacitor bank is located in a concrete lined pit approximately 13 feet by 10 feet by 8 feet deep which is electromagnetically hidden under a 16 foot by 32 foot copper ground plane which serves as the floor of the experimental area. Figure 6 is a plan view of the Facility showing the adjacent shielded enclosure which houses the instrumentation. An adjacent control cubicle houses the system controls, monitors, and trigger circuitry. The capacitors have an individual capacitance of 0.5 microfarad with a combined bank capacitance (four in parallel) of 2.0 microfarads. The maximum voltage rating is 125 KV with a 10 percent inverse voltage rating. Peak to peak voltage rating can occur during discharge when an initial charge voltage of 70 KV is used. The unit is, therefore, seldom charged above 70 KV unless appropriate damping is applied. A discharge tank assembly serves to interconnect the capacitors and to isolate the distribution plate and other high voltage elements in dielectric oil. It also provides

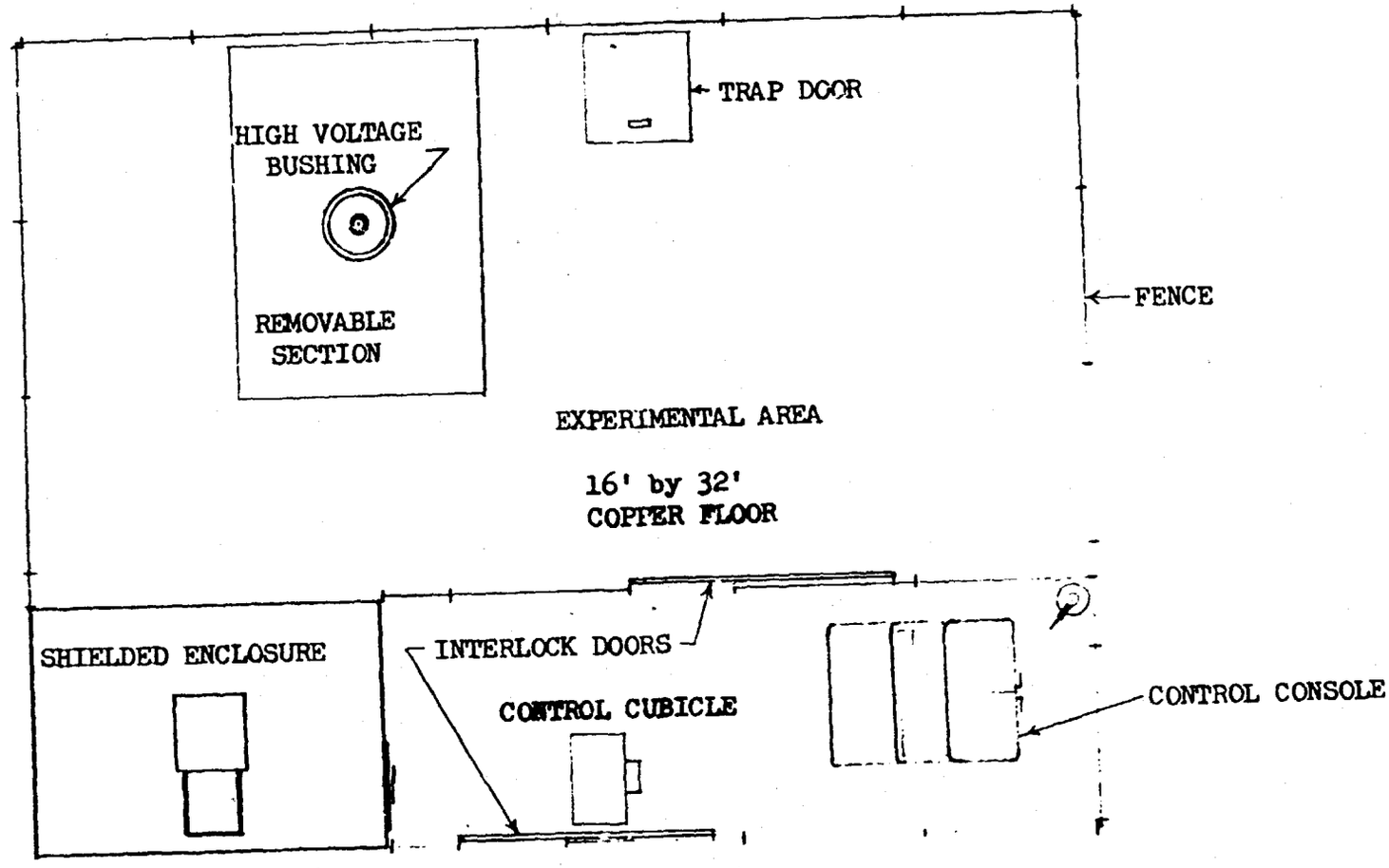

FIGURE 6 PLAN VIEW OF EMP EXPERIMENTAL FACILITY

a means of charging the capacitors through a limiting resistor, discharging them via a spark gap assembly and bleeding off the residual charge on the capacitors.

The high voltage charging supply used in this system is a Sorenson Corporation, Beta Model Number 2120-5. It is comprised of two units: the high voltage section housed in an oil filled 30 inch cubical metal tank and a control unit located in the control console. The high voltage section has a maximum output of 120 KV DC.

A bleed-off tank is installed in the high voltage input line in order to provide an external resistive path to ground when it is desired to discharge the capacitors. This unit is normally used to bleed off the residual charge after a discharge. A shorting bar within the discharge tank is delayed until the capacitor voltage is negligible, thus avoiding possible arcing and contamination of the insulating oil.

The spark gap assembly is a three electrode switch of modified EG&G design in which one of two large electrodes contains the trigger probe. Each large electrode consists of a stud type of contact of Elkonite mounted on a base section of stainless steel. The spacing between the electrodes is nominally 5/8 inch. The electrodes are held by a heavy nylon chamber that also isolates the gap from the discharge tank. The trigger probe is a 1/16 inch diameter tungsten wire, furnace brazed to a mounting flange. The gap is designed to operate at pressures of from one to two atmospheres. Water pumped nitrogen with 6% oxygen added is the usual gas mixture used in the chamber.

A control console located in the control cubicle adjacent to the experimental area contains the following equipment:

a. Fiducial Generator Panel

b. Closed Circuit TV Monitor Panel

c. Solenoid Monitor Panel

d. Intercom Panel

e. Gap Pressure Control Panel

f. Power Panel

g. High Voltage Control Panel

h. Trigger Control Panel

i. High Voltage Monitor

j. Interlock Panel

All instrumentation for the facility is located in a shielded enclosure located adjacent to the experimental area. The shielded enclosure is constructed of a single layer of 24 gauge cold rolled galvanized sheet steel. All seams are held together under pressure applied to mating surfaces of adjacent panels. All panels contain wood supports on the inside. The 10 feet by 7 feet by 8 feet high room has a 35-1/2 inch by 84 inch double door with two rows of heavy-duty spring bronze contact fingers mounted around the periphery.

Signal leads enter the shielded room through 8 RF feed-through connectors. The connectors are a waveguide beyond cut-off type and are bonded directly to the room. Power line filters are 0 to 400 cps bandpass, 20 amperes per filter. Air conditioning is

provided by a 25,000 BTU unit mounted on the roof of the room with air inlet and outlet via a waveguide type panel. The shielding effectiveness of the room determined experimentally is shown in Figure 7.

Read-out for the experimental facility is accomplished via oscilloscope camera combinations. Signal processing within the shielded enclosure before oscilloscope display is done with operational amplifiers and impedance transform equipment mounted on a relay rack adjacent to the oscilloscopes.

5. INSTRUMENTATION DEVELOPMENT

Precise and repeatable electromagnetic field measurements as a class are among the most difficult to perform, especially on a pulse basis where broad band data are desired. Extreme care is required in the design of the measurement equipment to limit the distortion of the fields being measured, minimize the noise in the data link and harden those ports of the equipment which are susceptible to the fields but not relatable to the measurement. In this section, various devices will be discussed which are consistent with the above constraints. Conceptually they fall into classes whereby either complete electromagnetic decoupling is accomplished in the frequency ranges of interest between the sensor and the receiver or sufficient signal strength and impedance transformation is provided at the sensor to dominate noise induced into cables.

5.1 Remote Signal Processing Amplifiers

Two electromagnetic environment hardened amplifiers

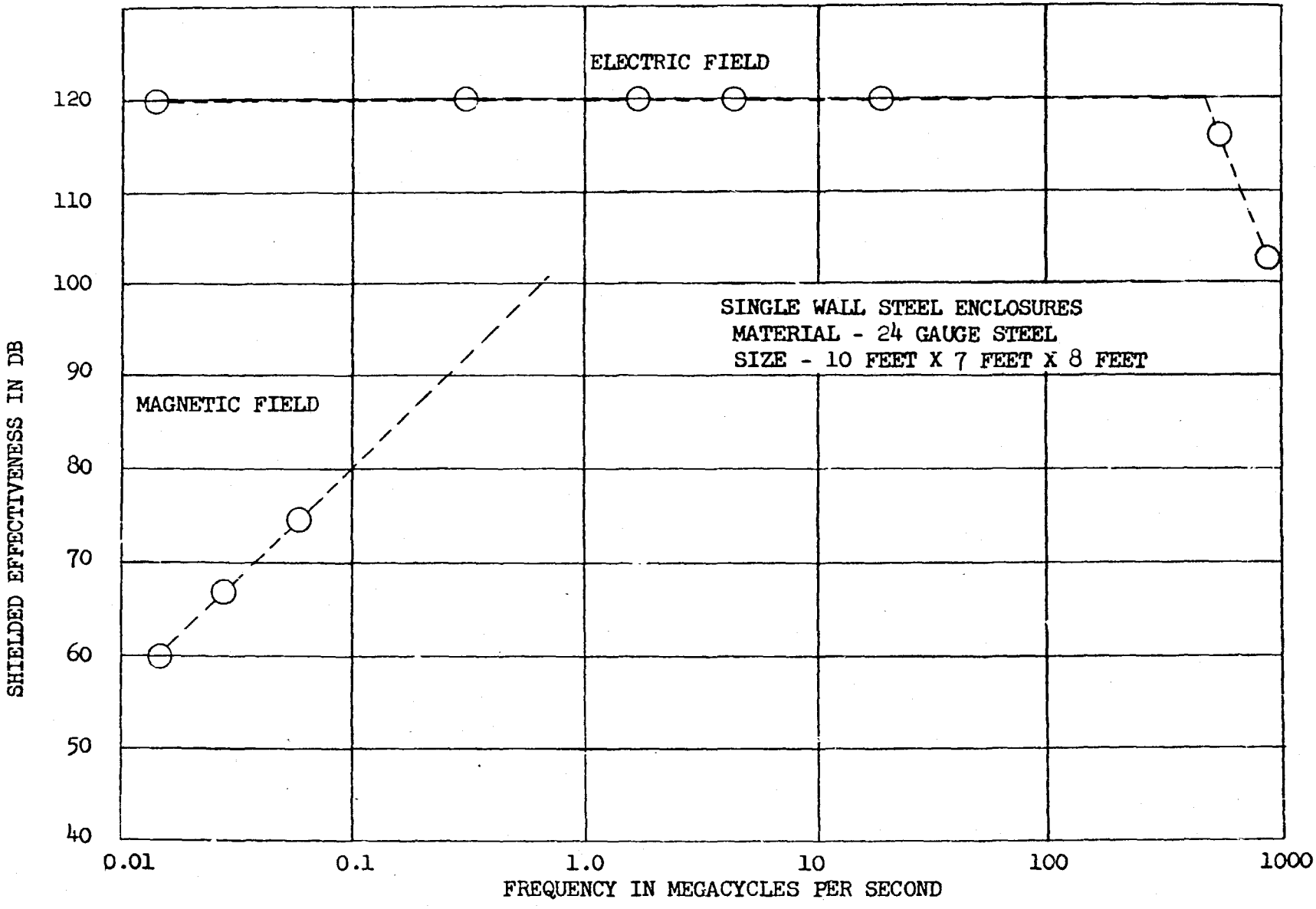

FIGURE 7 SHIELDED ROOM CHARACTERISTICS

have been developed for use in EMP experimentation. These amplifiers are differential throughout and incorporate low impedance output capabilities for driving long twinax cables. Input voltages are limited to a few millivolts. One of the amplifiers is shown in Figure 8 with a loop sensor attached.

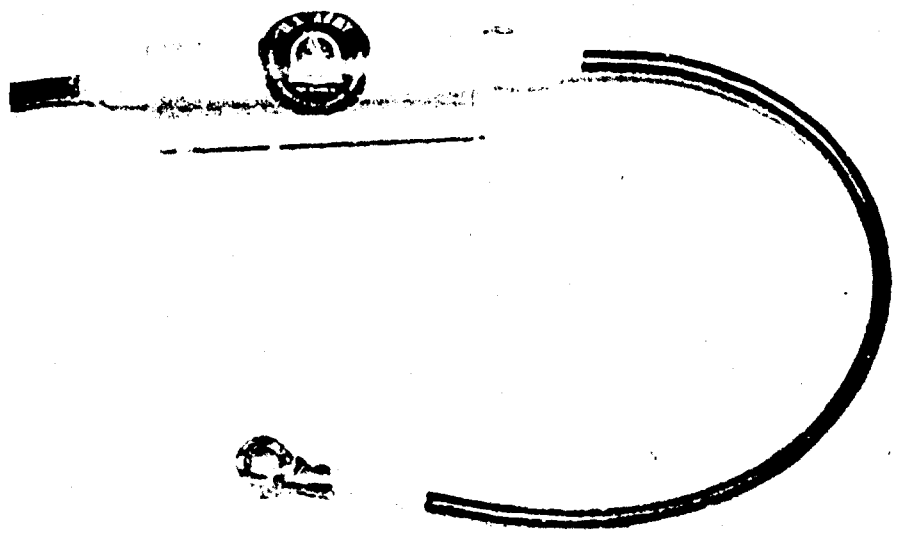

FIGURE 8 REMOTE SIGNAL PROCESSING AMPLIFIER

The amplifiers are mounted in 1/4 inch thick aluminum cans for

ruggedness and electromagnetic shielding. The circuitry is mounted on glass boards attached firmly within the can as shown in Figure 9.

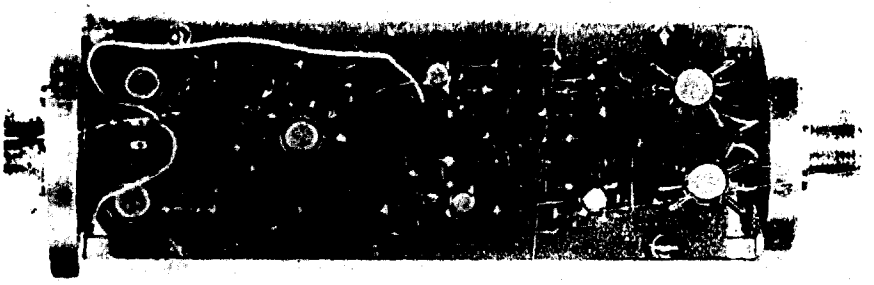

FIGURE 9 REMOTE AMPLIFIER CIRCUITRY

The basic circuit uses a Motorola MC 1519 integrated circuit of high gain and minimum unbalance characteristics. Two circuits are used, one a high gain amplifier with wide bandwidth capabilities and another with moderate gain and bandwidth capabilities.

5.1.1 High Gain Amplifier[4]

This unit is a 64 db amplifier with a judicious amount of feedback incorporated to obtain stability and high frequency response. The circuit schematic is shown in Figure 10. Input stages of the amplifiers are powered from an internal battery pack which has negligible current drain. The output stage is of a remote emitter follower design in which the emitter resistors are located at the read-out end of the instrumentation cable and are biased such that the instrumentation signal lines float at operating DC values. In this configuration, a DC power supply can be used at the read-out end of the instrumentation cable to supply the power consuming driver stage of the amplifer thereby eliminating the necessity for a large battery pack in the amplifier itself. Differential frequency response characteristics are shown in Figure 11.

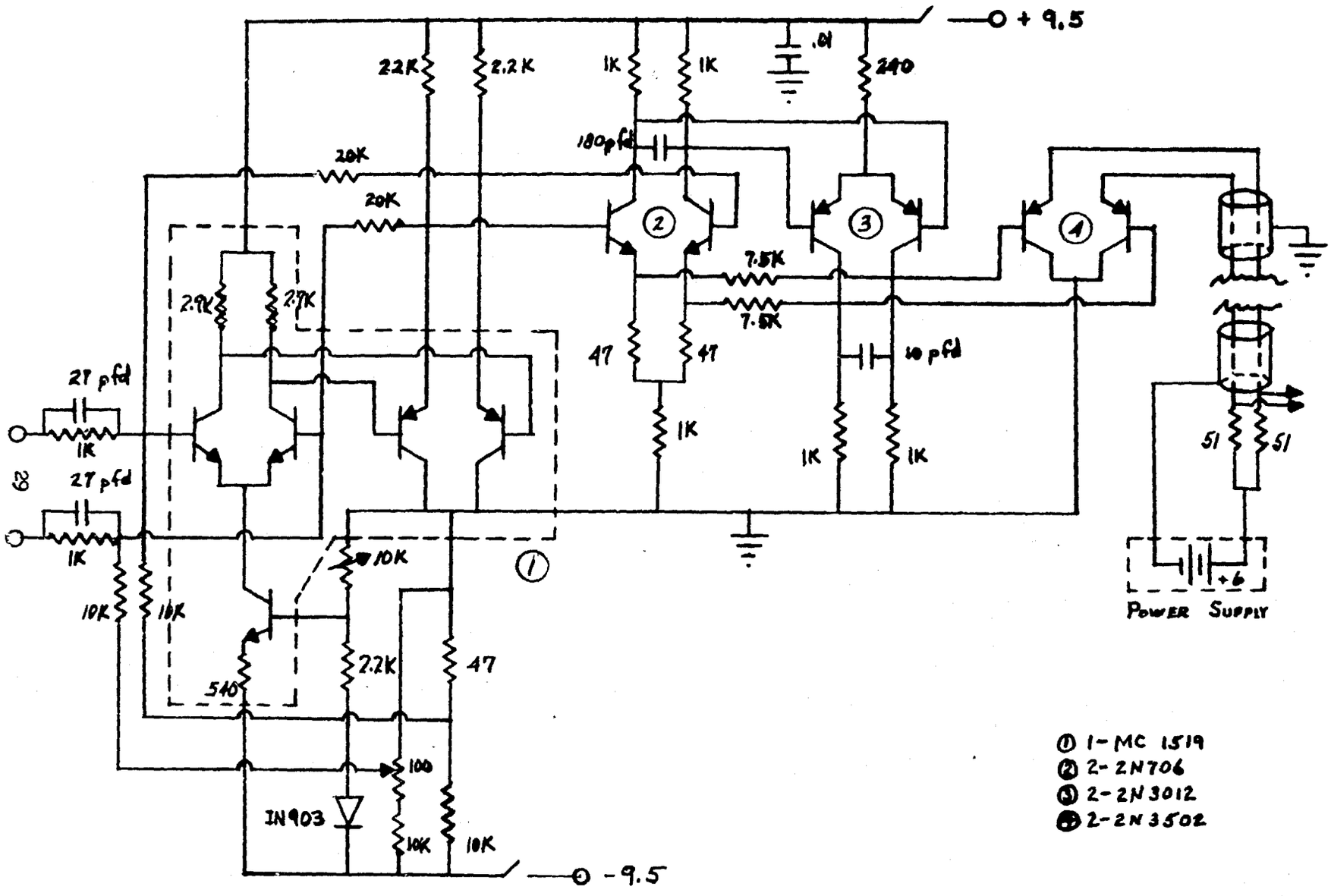

FIGURE 10 HIGH GAIN DIFFERENTIAL AMPLIFIER SCHEMATIC (U)

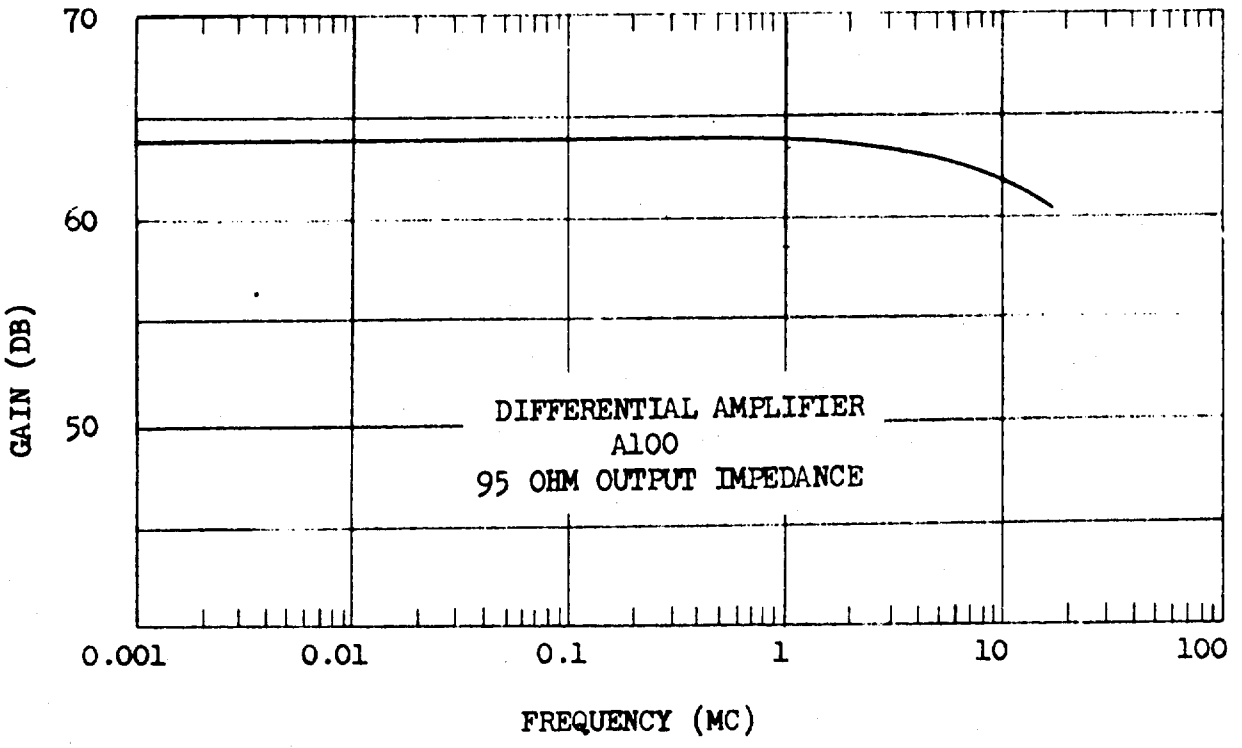

FIGURE 11 HIGH GAIN AMPLIFIER FREQUENCY RESPONSE

5.1.2 Moderate Gain Amplifier

This unit is a 40 db amplifier designed to be as simple as possible to eliminate noise sensitive elements. Active elements are limited to one Motorola MC 1519 integrated circuit. Bias is provided by internal battery and eight hours of continuous operation is possible on one set of batteries. The schematic is shown in Figure 12 and the frequency response in Figure 13.

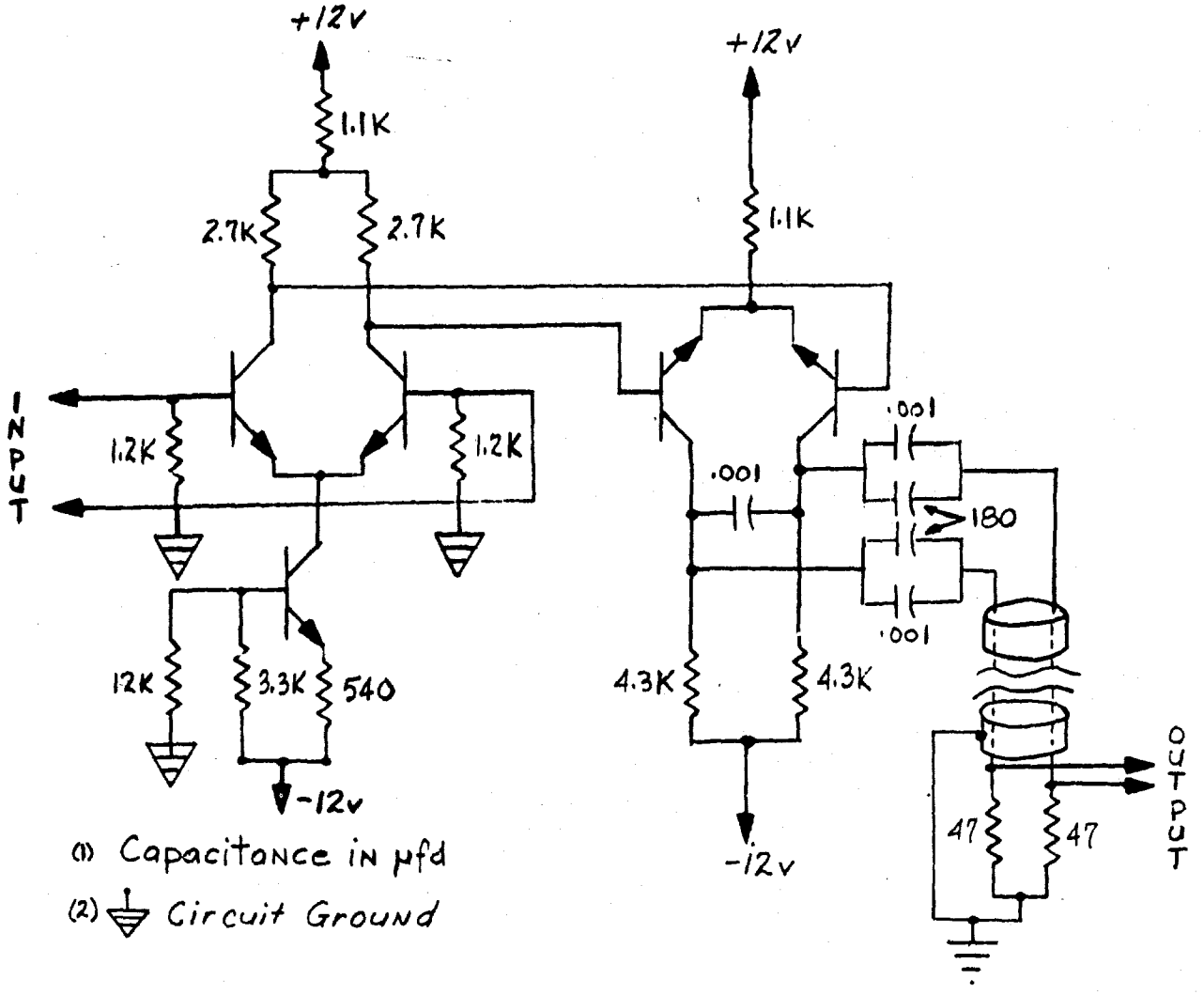

FIGURE 12 MODERATE GAIN AMPLIFIER SCHEMATIC

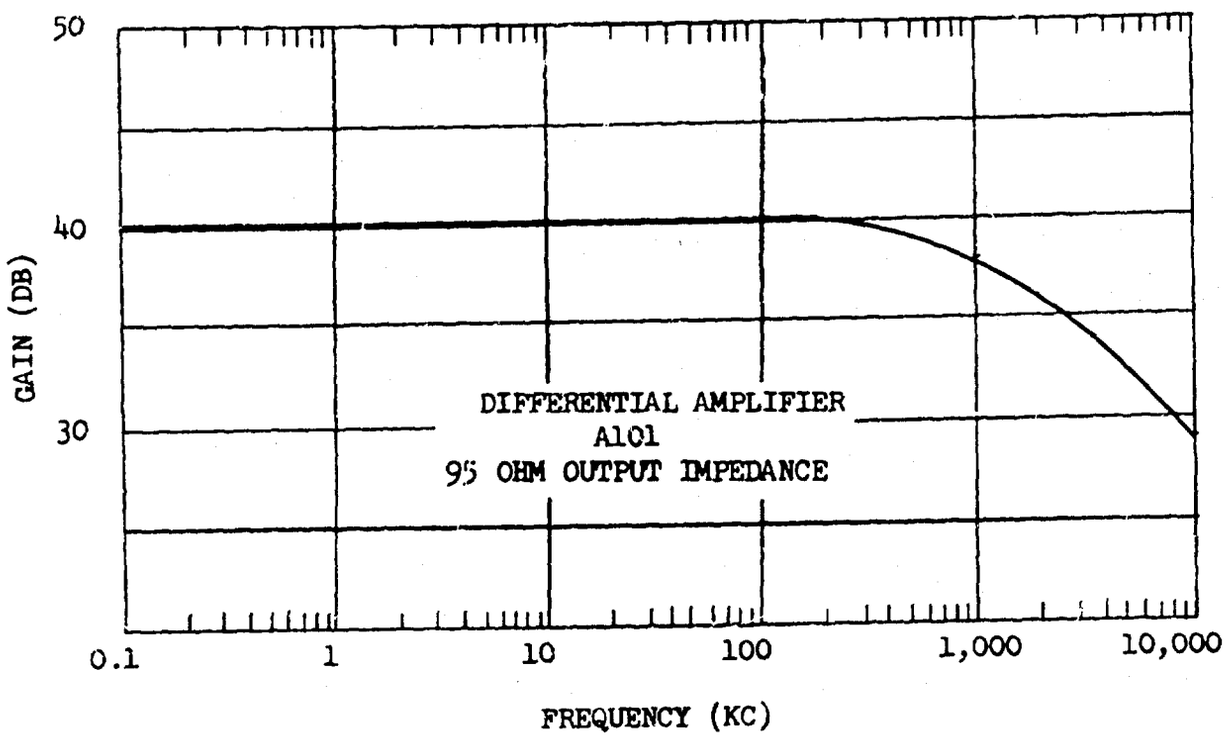

FIGURE 13 MODERATE GAIN AMPLIFIER FREQUENCY RESPONSE

5.2 Passive Birefringent Crystal Field Sensors

An optical data link and compatible field sensor has been developed[5] which operates principally above visible light frequencies and uses a completely passive sensing element. The sensing element is a birefringent crystal which changes from uniazial upon application of an electric field. A similar sensor has been designed for magnetic field measurement using the Faraday

rotation which a diamagnetic glass in a magnetic field imposes on a light beam.

5.2.1 Electric Field Sensor

The largest electro-optic effect in applicable crystals is obtained when the electric field and the light beam are in parallel to the Z axis of the crystal. When an electric field is applied in the Z direction, the orthogonal optic X and Y axes are rotated by 45 degrees. This angle is independent of magnitude of electric field. If then randomly polarized light is sent through the crystal in the Z direction, the velocity of the components along the rotated X and Y axis becomes a function of the applied field. The rotation or difference in the index of refraction is called the birefringence. Birefringence is directly proportional to the cube of the ordinary index of refraction, a constant describing the birefringency or Pockels effect and the electric field. When the field is zero, the birefringency is zero.

Sending linearly polarized light through the crystal with the polarization along the rotated X or Y axis will cause relative phase shift of the components. In general, these orthogonal components shifted relatively in phase will produce elliptically polarized waves. That is to say, the application of an electric field or a voltage across the crystal will change the linearly polarized light to elliptically polarized light. Passing this light through another polarizer or analyzer will cause the output light to be a function of the described ellipse.

The relative transmission of light through the above system is, therefore, a function of the applied voltage (or electric field) across the crystal and the constants of the crystal. With the polarizers crossed as shown in Figure 14, it is possible to lump

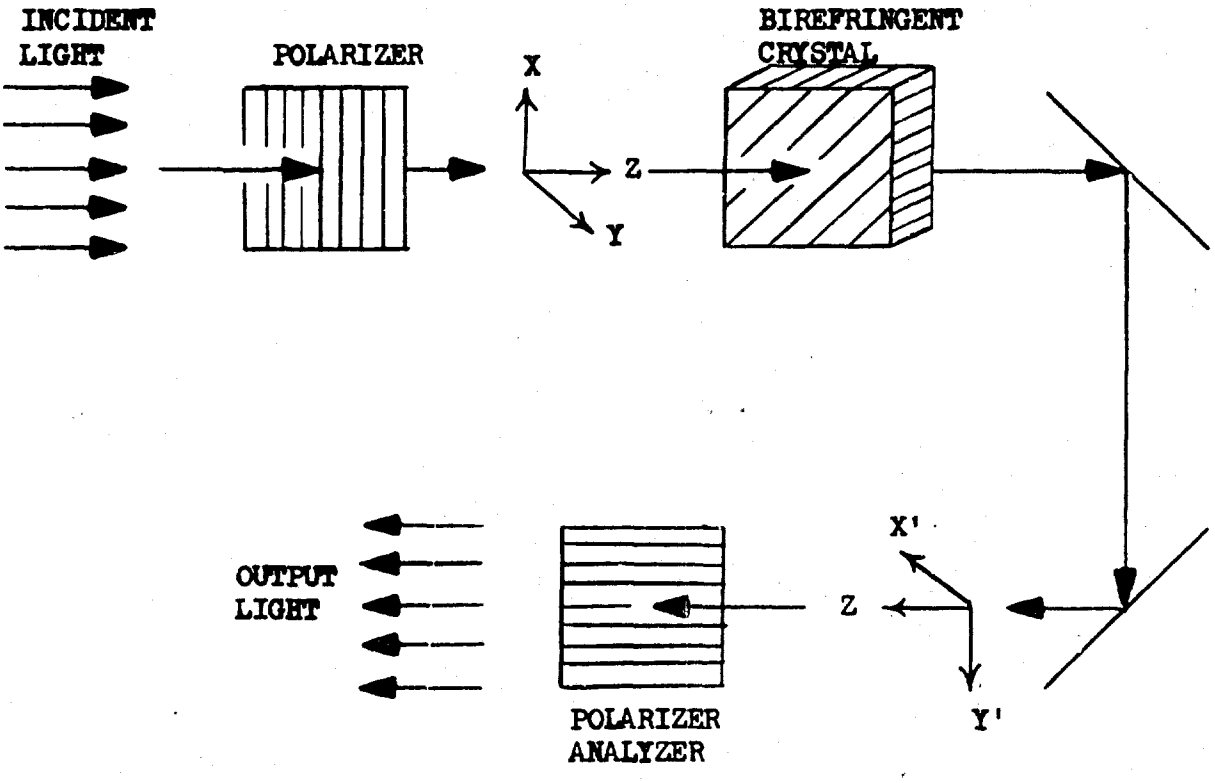

FIGURE 14 SIMPLE ELECTRO-OPTIC SYSTEM

all the constants together as a half wave retardation voltage. Namely

$$T = \sin^2 \frac{\pi}{2} \frac{V}{V_{\lambda/2}} \qquad (2)$$

where T is the relative transmission of light, V is the applied voltage, and $V_{\lambda/2}$ is the half wave retardation voltage. From a curve of this type as shown in Figure 15 and the drive voltage, one can determine the waveshape of the amplitude modulated light output.

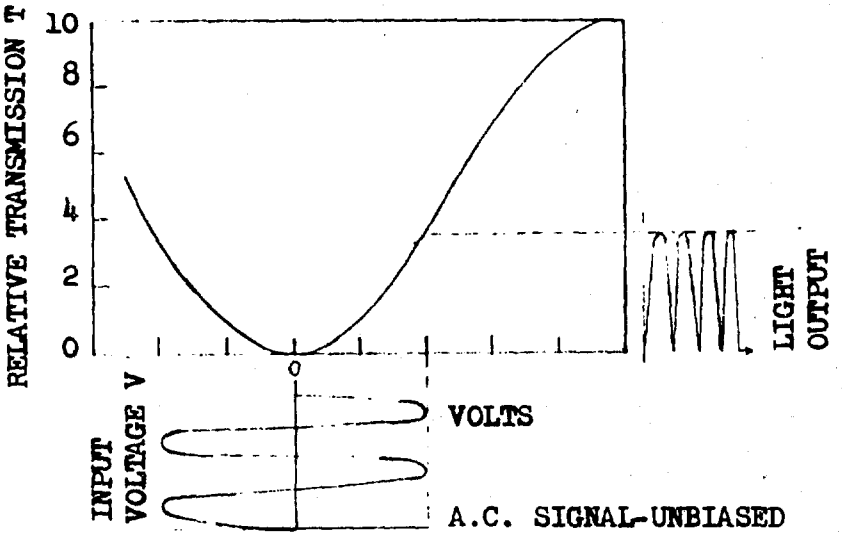

FIGURE 15 UNBIASED ELECTRO-OPTIC SYSTEM

For crossed polarizers as described one can see that the response of the system is non-linear and that principally second harmonic or, in general, even harmonic light outputs are obtained. To obtain a linear responding system desirable for analog data handling, one must apply a bias to shift the response curve to a linear response region as shown in Figure 16.

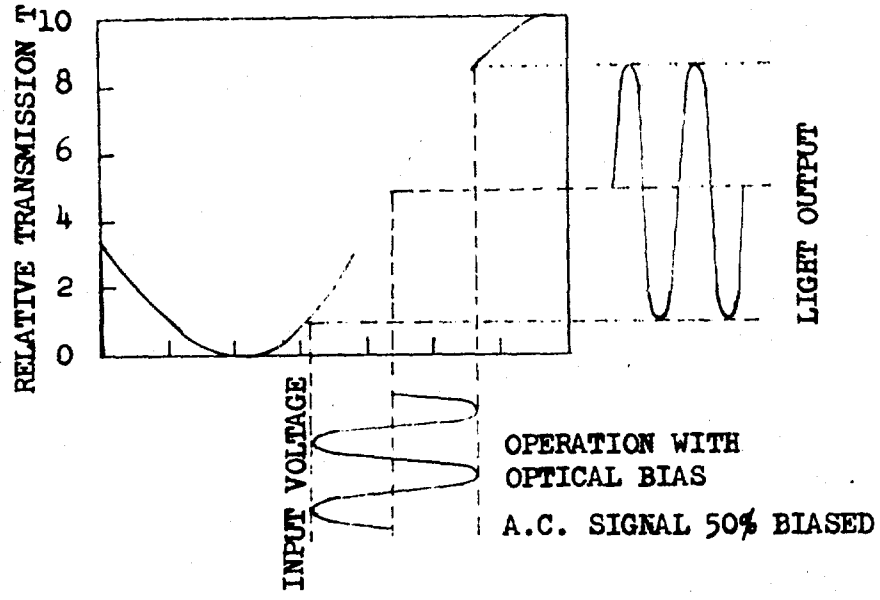

FIGURE 16 BIASED ELECTRO-OPTIC SYSTEM

Although a voltage bias on the crystal can be used, a more simple approach would be the insertion of a quarter wave retardation plate. This simple addition results in a 50 percent of maximum bias which

automatically sets the operating point of the system to the most linear region of the response curve provided the driving voltage is kept small (plus or minus 30 percent of maximum response about the bias point). Increased driving voltages will subsequently increase the third harmonic distortion of the system.

Several crystals of the 42m or D_{2d} tetragonal scalenohedral class have electro-optic responses as described. Two such crystals with large low frequency Pockels constants are ammonium dihydrogen phosphate (ADP) with a half wave voltage of 9.3 kilovolts at 5500A° and potassium dihydrogen phosphate (KDP) with a half wave voltage of 7.7 kilovolts at 5500A°. These half wave voltages are determined by a direct effect which involves interaction between electron clouds and the applied field and by an indirect effect involving the mechanical resonances of the crystal, a function of its dimensions. These mechanical resonances will give many times the stated responses at resonant frequencies; however, by mechanical clamping the lower frequency responses of KDP can be controlled to about 10 percent and ADP to about 40 percent as shown in Figure 17. The break points shown are illustrative only and are determined by the crystals aross-sectional dimensions.

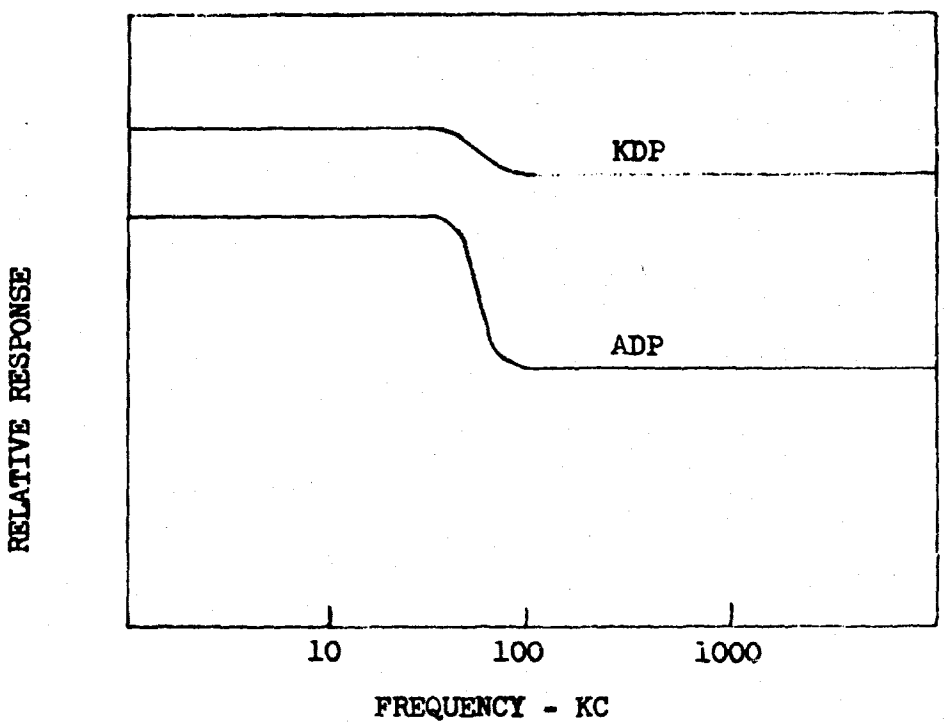

FIGURE 17 CLAMPED CRYSTAL RESPONSE

The electric field sensors described herein use KDP as the crystal element for a number of reasons. One principal reason involves the lower mechanical resonance effect of a clamped KDP crystal as opposed to that of the ADP crystal. Other reasons involve expediency and are not necessarily scientific in nature.

One important consideration which is of prime importance in choosing a usable crystal is that of half wave retardation voltage, for the lower this voltage, by definition, the

more sensitive the crystal. This half wave voltage is a linear function of the light frequency being used as shown in Figure 18.

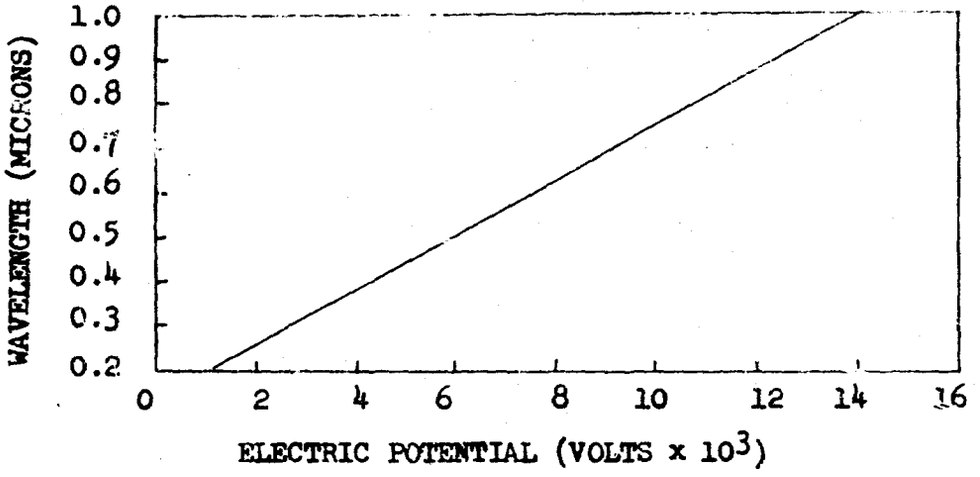

FIGURE 18 BIREFRINGENCY RESPONSE OF KDP

It is, therefore, advantageous to choose a light source containing short wavelength light components. Monochromatic light, although theoretically cleaner to analyze, is not necessary, however, since a weighted average of all the light frequency source components can

be used. In addition, one must consider the integrated system transmission at various light frequencies.

The physical arrangement chosen for the electric field sensor was dictated by the expected use of the device. It was desired to maintain both the light source and the light receiver at the same location in order to minimize ground loops in the circuitry and to localize the equipment for ease of operation. For these reasons, a mirrored surface was deposited on one side of the crystal to which was fitted a thin metallic ring serving as one electrode. A gold annular film was deposited on the opposite face with a metallic ring to form the other electrode. A 1/4 inch diameter window was masked off from the gold deposit to form the sensor aperture. The polarized light beam, therefore, makes a double pass through the crystal. For minimum light absorption and ease of light beam orientation, a crystal of 0.10 inches thickness was chosen. The path length through the crystal is therefore 0.20 inches.

The sensor package consisting of the crystal and the electrodes was placed between two glass slides and clamped in an acrylic housing to dampen out the mechanical resonances. The acrylic housing was fastened into a rectangular acrylic block as shown in Figure 19 with adjustment screws to permit orienting the crystal when the block was firmly attached in measurement position.

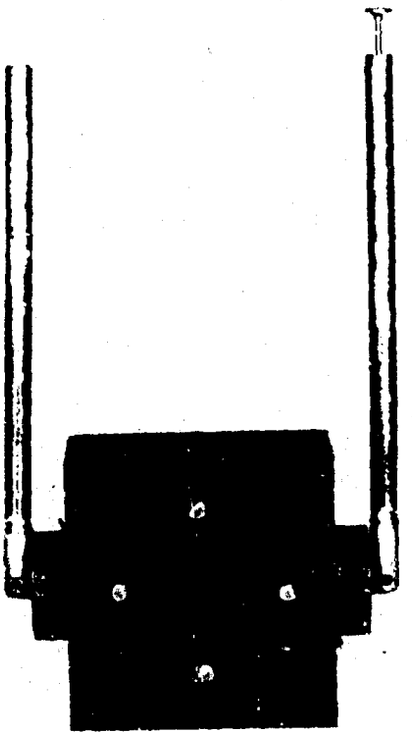

FIGURE 19 ELECTRIC FIELD SENSOR

Two telescoping rods mounted on the block serve as the sensing elements. Each rod is adjustable from approximately 10 cm to 1 meter and is hinged to give 2 π coverage. The effective height of this dipole is electrically short for wavelengths of interest.

5.2.2 Light Transceiver

Figure 20 shows the arrangement used to supply light to the electric field sensor, receive the amplitude modulated light, and convert amplitude modulated light to an electrical signal. In the design of the system, consideration was given to the relative response of the various components as a function of light wavelength. Figure 21 shows these responses on a common graph. A mercury light source was chosen because of its high output at short wavelengths within the band-pass of the KDP crystal.

A 100 watt mercury lamp is used to obtain sufficient ultraviolet light output. The photomultiplier tube chosen to read the light modulation is a 1P28 with an S-5 response peaked in the ultraviolet region as shown. Photodiodes were preferred for circuit simplicity but were not sufficiently sensitive at the light frequencies involved. Figure 22 is a picture of the system as used in the field.

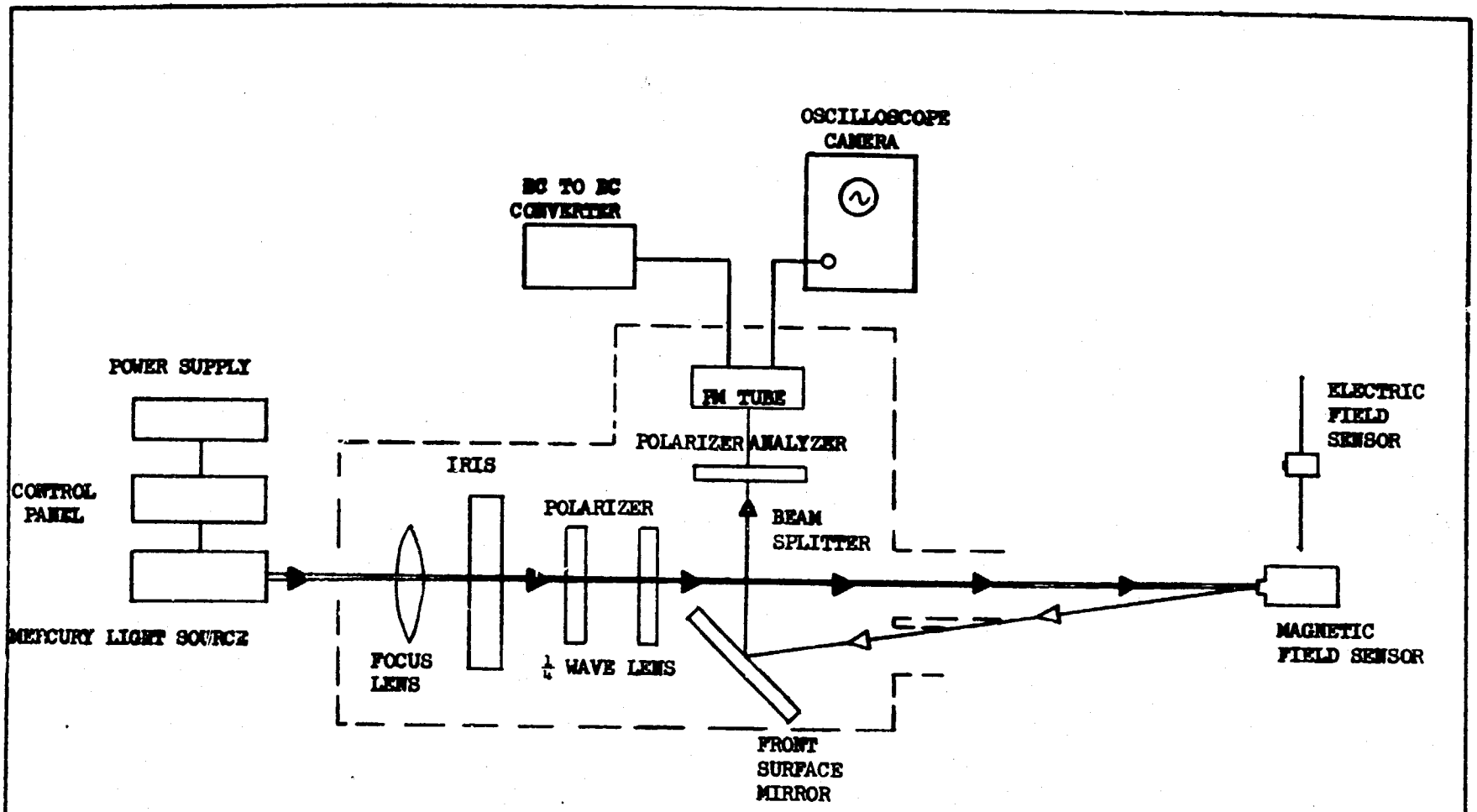

FIGURE 20 LIGHT TRANSCEIVER

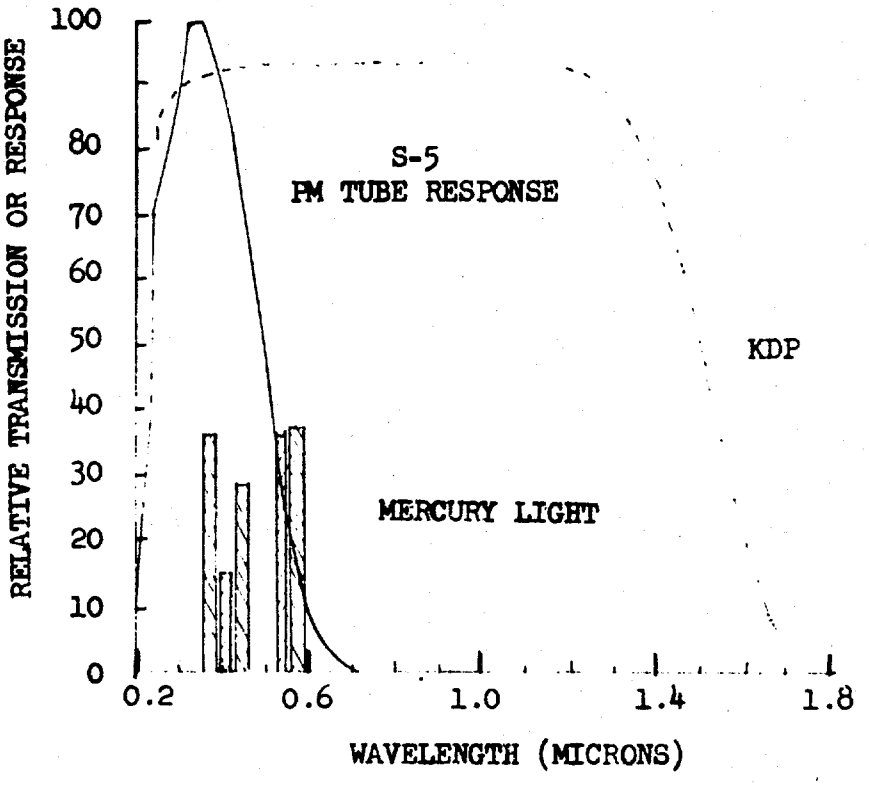

FIGURE 21 SYSTEM LIGHT RESPONSE

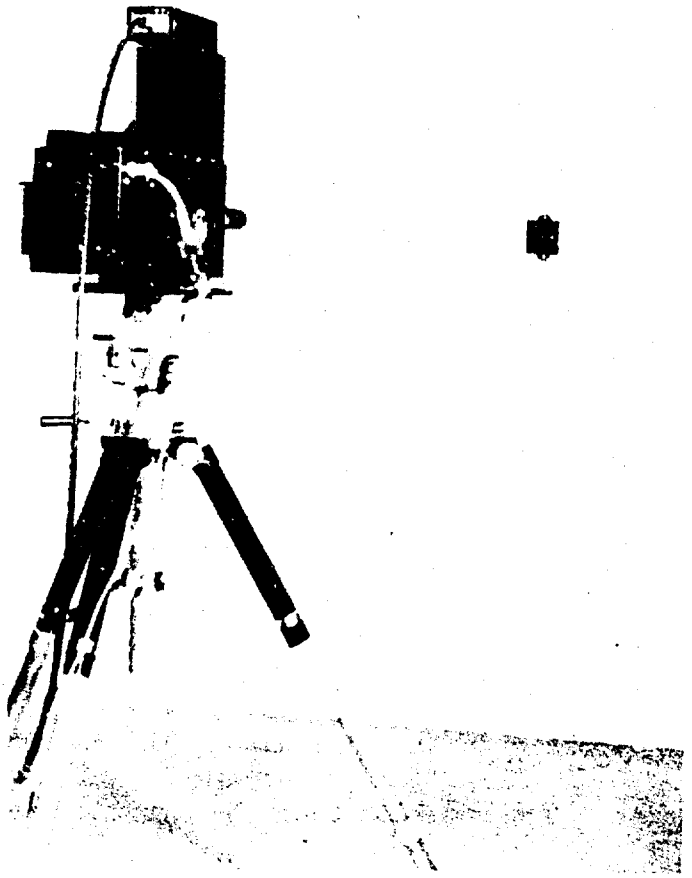

FIGURE 22 ELECTRIC FIELD SENSOR SYSTEM

5.2.3 Magnetic Field Sensors

Using a similar system to that delineated for electric field sensing, a corollary magnetic field sensing system has been developed. As in the electric field sensor, a linearly polarized light beam is passed through a solid in the direction of the magnetic field where a rotation associated with circular birefringence is developed. The amount of rotation is given by

$$\theta = VBl \qquad (3)$$

where θ is the amount of rotation in degrees, B is the magnetic field in Gauss, V is the constant associated with the birefringency or the Verdet constant, and l is the length of the solid.

Although the response of this system is, in general, as described for the electric field sensor, the system can be simplified due to the small rotations involved at field levels of interest. That is to say, for small variations of the angle the sine of θ is approximately equal to θ. For the solid chosen which is a diamagnetic dense flint glass, the Verdet constant is 0.1 minutes/cm-Gauss. The rotation over the dynamic range of interest is less than one degree and the above approximation is certainly valid. In this case, bias to the system is obtained by crossing the polarizers at 45° to eliminate even harmonics.

The magnetic field sensor shown in Figure 23 consists of a dense flint glass cylinder three inches in length,

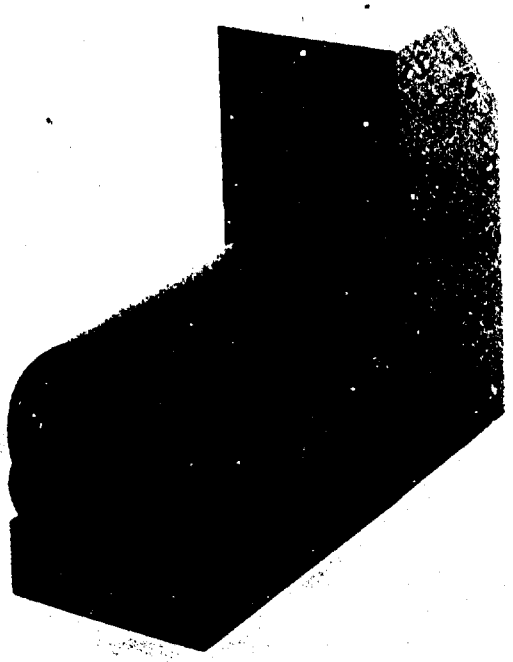

FIGURE 23 MAGNETIC FIELD SENSOR

mounted in an acrylic block. One face of the cylinder has an anti-reflection coating. The other face is open to a set of front surface mirrors which reflect the light back to the light transceiver. The light transceiver is identical to that used for the electric field sensing system with the exclusion of the 1/4 wave plate which is no longer necessary for optical biasing.

5.2.4 System Characteristics

The characteristics of the birefringent crystal field sensors are largely a function of the particular application. The degree of alignment, separation of elements, ambient light, etc. all effect the calibration of the device. However, a minimum specification can be presented. Use in the field requires a calibration after set up at one given frequency and amplitude to provide meaningful data.

a. Amplitude Measurements: The magnetic field sensors can be used to take meaningful measurements from 20 gauss to 100 gauss. The electric field sensors can be used to take meaningful measurements from 500 volts per meter to 10^5 volts per meter.

b. Bandwidth: The bandwidth is purposely limited to DC to 10 megacycles per second in order to obtain adequate signal to noise ratios.

c. Signal to Noise Ratio: Minimum signal to noise ratios of 20 db have been established.

d. Input Impedance: The input impedance of the electric field sensor is greater than 10 megohms resistive, approximately

3 picafarads at the crystal and approximately 15 picafarads at the dipoles. The input impedance of the magnetic field sensor is undetermined.

e. Power Requirements: Sixty volts, 10 amperes, direct current for the mercury light source and a one kilovolt DC to DC converter for the photomultiplier independent of utility lines are supplied.

f. Dimensions: The magnetic field sensors are cylindrical with a diameter of two inches and a length of six inches. The electric field sensors are in the form of a rectangular prism with two dipole antennas extendable from 0.1 meter to one meter each. The trensceiver is irregular in shape and approximately 12 inches in its maximum dimension.

g. Construction: The field sensors are enclosed in non-metallic containers, sealed from any dust which might be present under field conditions. The transceivers are housed in light-tight anodized aluminum containers and are mounted on tripods.

h. Controls: On-off switches are provided for the light source and photomultipliers. Momentary high voltage switches to start the light source and mechanical adjustments for the transceiver optics are available.

5.3 Active Fiber-Optical Field Sensors

5.3.1 Description of the Sensor

A multirange electric field sensor has been developed[6] that incorporates a fiber optic transmission link between

the field measuring point and the light receiver. Capabilities of the sensor include frequency response from 135 cycles per second to 1 megacycle per second and field levels of 0.030 volt per meter to 300 kilovolts per meter through the use of a sensitivity switch. The detector is battery powered and no electrical connection is made between the sensor and the read-out instrumentation. This system eliminates the field distortions normally caused by conducting cables and also eliminates the cable noise difficulties inherent with hard wire data transmission systems.

Two units (a detector and a receiver) coupled by a length of non-coherent glass fiber optic light guide comprise an electric field sensor as shown in Figure 24.

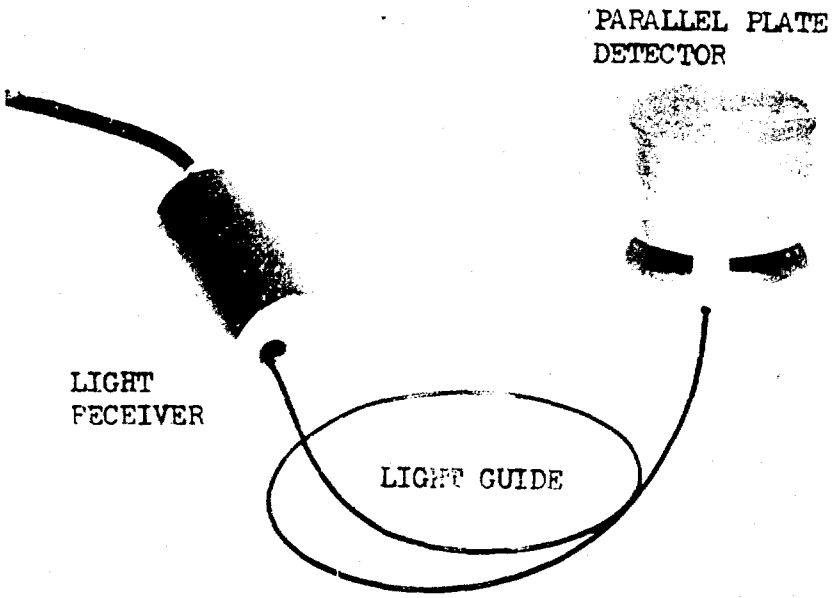

FIGURE 24 ELECTRIC FIELD SENSOR

The detector consists of a parallel plate antenna and a preamplifier driving a gallium arsenide light emitting diode for light transmission into the light guide. Location of the electronics and the battery is within a cylinder which comprises one of the plates of the parallel plate antenna as shown in Figure 25.

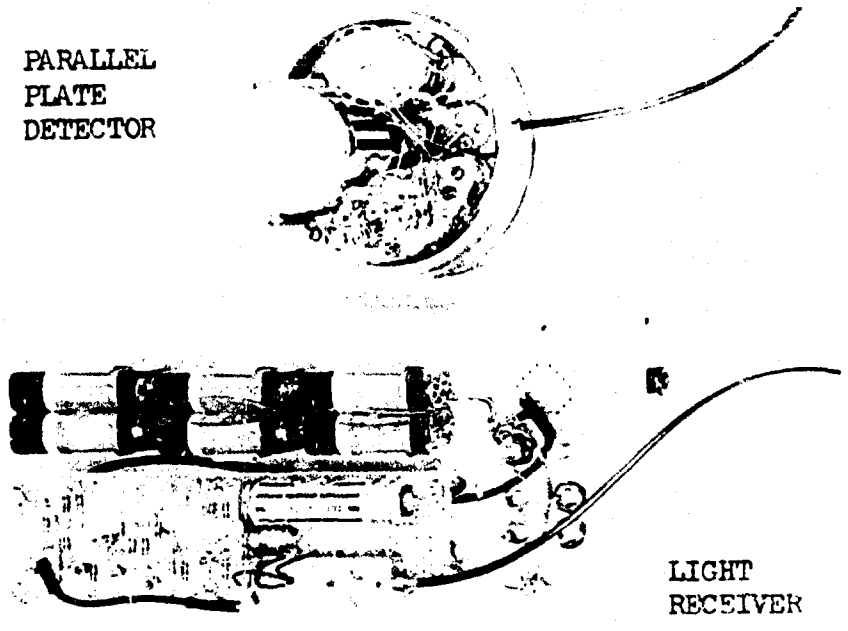

FIGURE 25 PARALLEL PLATE ANTENNA

The receiver consists of a photo-diode detector for light demodulation followed by a low noise amplifier with low impedance output to drive instrumentation cables which are terminated at the data recording equipment. Transient electric field measurements are normally displayed on oscilloscope-camera units located in a shielded instrumentation enclosure. Up to 24 feet of light guide

The detector consists of a parallel plate antenna and a preamplifier driving a gallium arsenide light emitting diode for light transmission into the light guide. Location of the electronics and the battery is within a cylinder which comprises one of the plates of the parallel plate antenna as shown in Figure 25 .

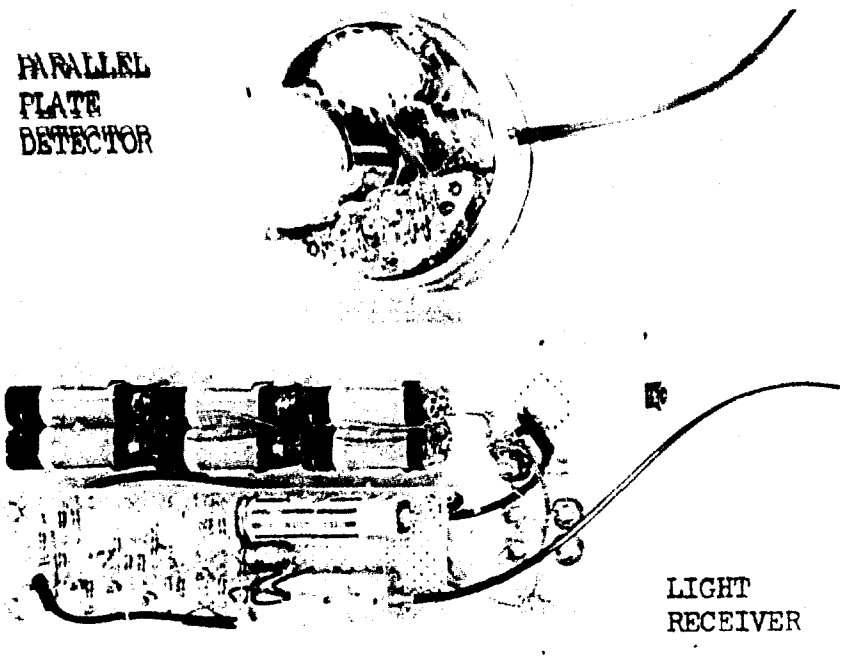

FIGURE 25 PARALLEL PLATE ANTENNA

The receiver consists of a photo-diode detector for light demodulation followed by a low noise amplifier with low impedance output to drive instrumentation cables which are terminated at the data recording equipment. Transient electric field measurements are normally displayed on oscilloscope-camera units located in a shielded instrumentation enclosure. Up to 24 feet of light guide

has been used between the parallel plate detector and the light receiver. The receiver has been used in the field to drive up to 100 feet of shielded cable and acceptable noise levels were maintained.

5.3.2 Parallel Plate Detector

The means devised for sensing the electric field is through the use of a parallel plate antenna with effective height of approximately 2 inches. This antenna which exhibits approximately 3 picafarads of capacitance is coupled to a very high input impedance, small geometry, field effect transistor. The input characteristics of the transistor provide a good match to the antenna and minimize loading which would seriously complicate the reconstruction of the true electric field. The output load of the preamplifier is a non-linear, low impedance, light emitting photo diode. This diode releases one photon for each 1,000 electrons; the photon energy is concentrated in the infrared region at a wavelength of 0.9 micron.

The detector exhibits directional response and to measure a specific orientation of electric field, the antenna plates are positioned such that the desired component is normal to the plane of the plates. With the plates in a horizontal plane, a vertical electric field component of 0.85 volt per meter yield the maximum voltage output swing (1.5 volts) allowable from the detector for the most sensitive attenuator setting at the detector. This voltage swing gives maximum light modulation. A dynamic range of 60 db allows measurements to 0.850 millivolt per meter for the smallest measurable field. In practice, however, the use of long light guides

reduces the dynamic range of the system to about 40 db; thus, the measurement range on the low end is 8.5 millivolts per meter.

Referring to Figure 26, the antenna signal is coupled through C1 into Q1, the field effect transistor, used in a source follower configuration. The bias on Q1 is determined by the voltage divider R1 and R2. Current through Q1 is determined by the value of R5. The voltage gain of this stage is only 0.8; however, the power gain is quite high since this stage exhibits very high imput impedance and a much lower output impedance.

In the most sensitive attenuator position, an additional amplifier stage, Q2 and Q3, are brought into the pre-amplifier operation. This essentially increases the voltage gain a factor of ten. When Q2 and Q3 are not in the circuit R11 and R12 provide the proper bias for the following stage. C8 is used to by-pass the AC signal around R11. Selection of C10 and C11 was made to obtain flat frequency response characteristics.

Q4 and Q5 is the principal amplifying stage with a voltage gain of 15 in switch positions 6 and 7. C12 by-passes the signal through R19 and C11 in these positions. In all other switch positions, these components are not by-passed and the gain is 1.5 for this stage.

The output stage, Q7, is a current source for the light emitting diode CR1. This current is determined by the ratio of the emitter voltage and R21. The emitter voltage is proportional to the input from the parallel plate antenna. Then from the

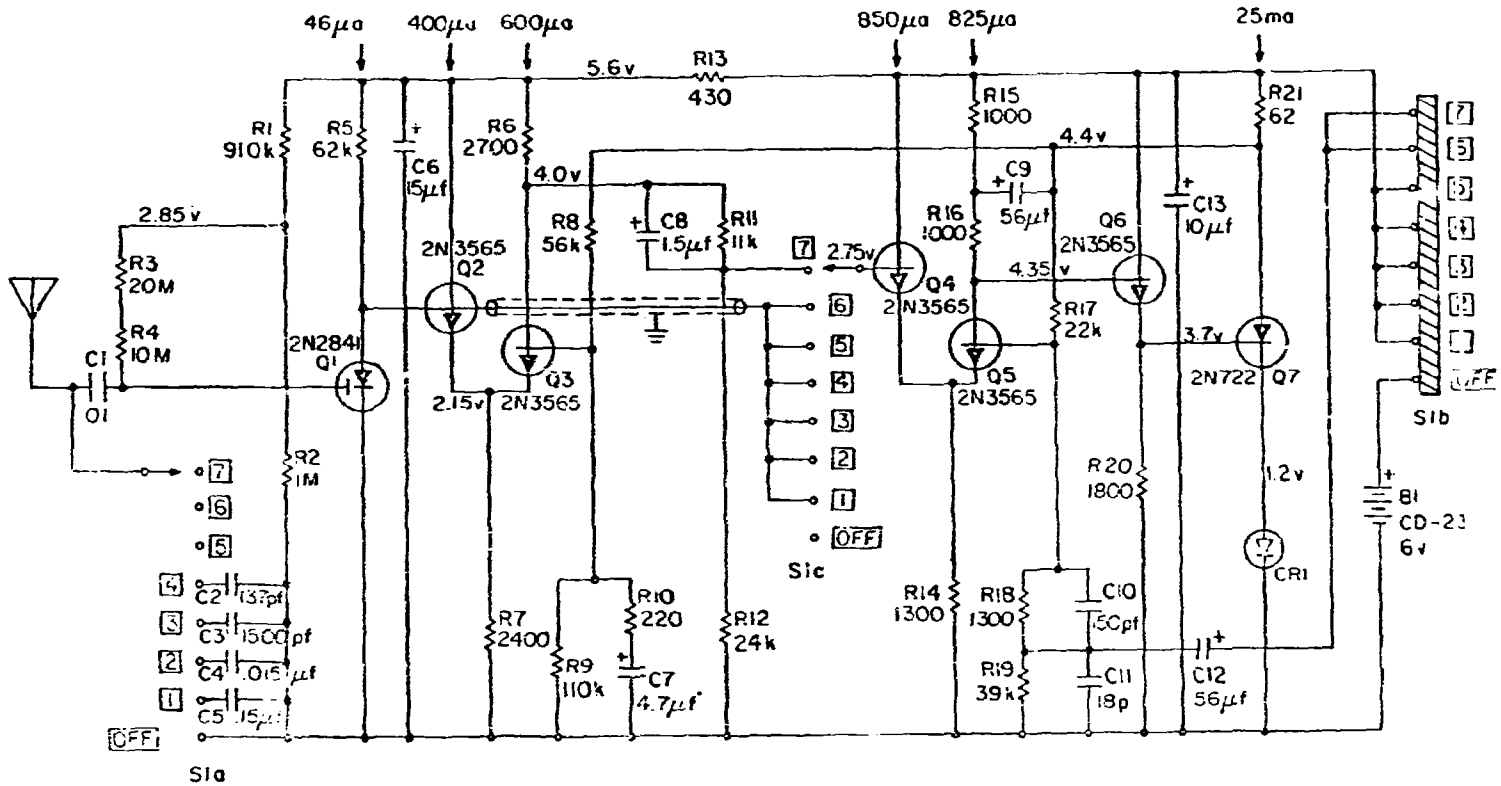

FIGURE 26 PARALLEL PLATE DETECTOR

diode, CR1, there is obtained the intensity-modulated light output, which is proportional to the measured electric field.

5.3.3 Light Receiver Description

The light receiver consists of a light detector (PIN photodiode) feeding a low noise, sensitive current amplifier. The signal from the photodiode is a current proportional to the photon flux rate incident on the photo-sensitive area of the diode. This photon flux rate, transmitted via the light guide, is proportional to the electric field incident upon the detector plates.

The signal current from CR1 is coupled to the field effect transistor as shown in Figure 27 which exhibits a high input impedance. The compound stage of Q1 and Q2 gives unity gain, low output impedance, and frequency response to 2 megacycles per second. Q3 gives a gain of 5, determined by the ratio of R7 and R8 (in parallel) with R6. The longtail pair amplifier consisting of Q4 and Q5 give a gain of 10.1 as determined from the ratio of R12 plus R15 to R15. The output stage provides a low impedance via a common emitter configuration. A peak periodic current of 5 milliamperes and peak periodic voltage swing of 5 volts are available at the output.

The voltage gain in the amplifier is 50 as determined by the gain of Q3, Q4 and Q5. The equivalent input impedance is 40 kilohms determined by the ratio of the feedback resistance (2M Ω) and the voltage gain.

Battery drain on B1 is so small that shelf life will determine its replacement. B2, however, supplies 8 ma of current

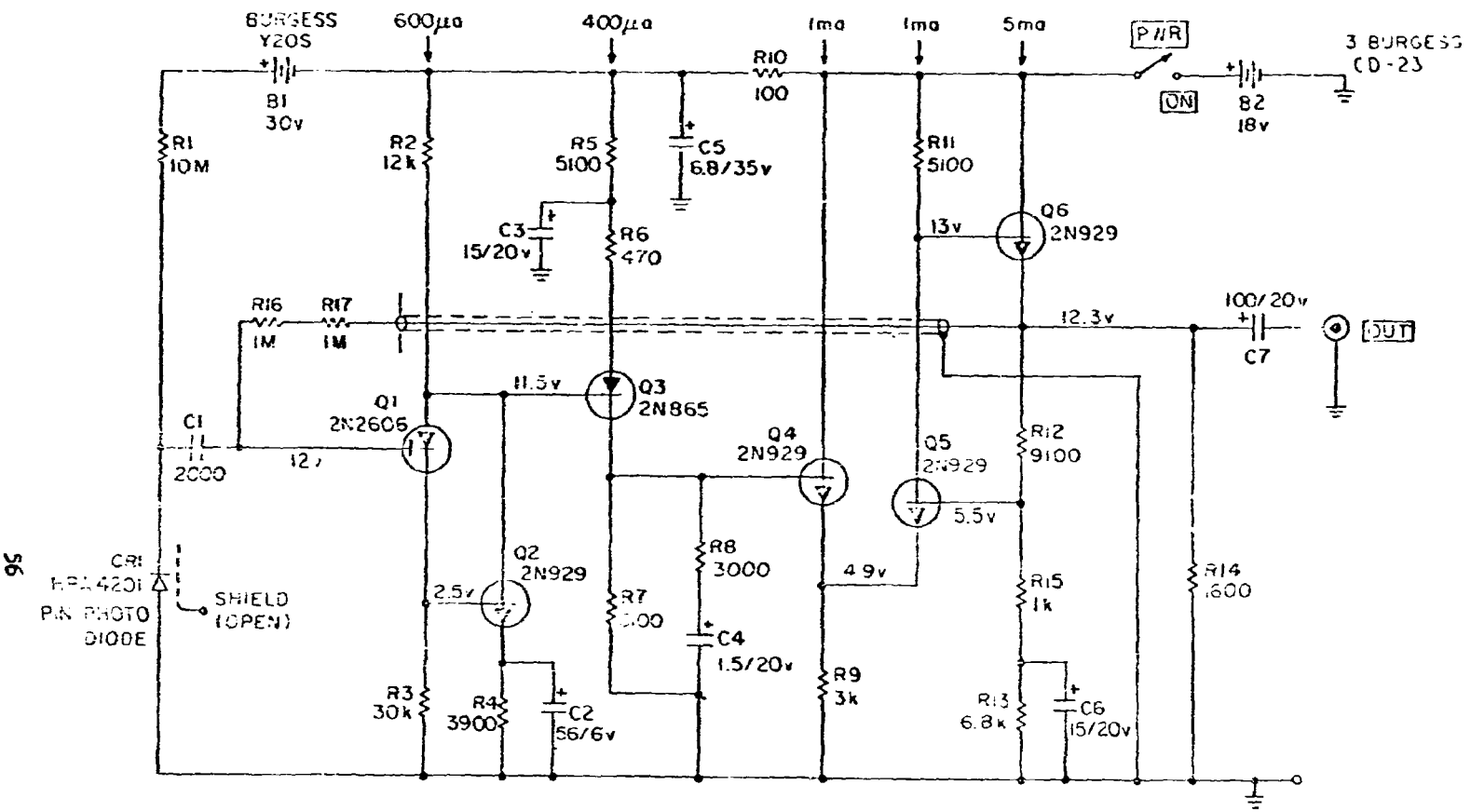

FIGURE 27 ELECTRIC FIELD LIGHT RECEIVER

and for 450 milliampere-hour operation will not need replacement or recharging for 64 hours.

5.3.4 Calibration

The complicated geometry of the detector makes it impossible to calculate the effective height of the parallel plate detector accurately. The technique used to determine the overall response of the sensor at various sensitivity settings was to place it in a known electric field environment generated by a large, parallel plate antenna as shown in Figure 28.

FIGURE 28 SENSOR CALIBRATION FACILITY

The calibration field is generated by applying a voltage between a 9 square meter screen and a copper ground plane. The plate separation is 1 meter; thus, the vertical electric field

in volts per meter is numerically equal to the plate voltage. Calibration is required only on sensitivity position 4, 5, 6, and 7 since the attenuator settings on positions 1, 2, 3, and 4 can be determined by injection of a signal directly into the sensor through a capacitor small compared to the shunt capacitor. A typical response curve is shown in Figure 29 for sensitivity ranges 1 through 7, and typical frequency response as measured on position 4. In many instances the use of a wave analyzer or any narrow band filter is a great help in increasing the measurement accuracy at the high sensitivity settings since the presence of stray fields incident upon the parallel plates are typically the same order of magnitude as the applied field.

The straightforward peak-to-peak readings from an oscilloscope display give sufficiently accurate readings for calibration of the sensor on all sensitivity ranges other than 6 and 7.

5.4 Loop Magnetic Field Sensor

5.4.1 Application

The peak amplitudes of transient magnetic fields to be measured in most experimental configurations range from fractions of a gauss to hundreds of gauss and the majority of the energy content is from 10 cycles per second to 1 megacycle per second; instrumentation must be compatible with these requirements. For measurement of the high level applied field generated within the EMP Experimental Facility, a loop sensor directly drives a terminated, twinax cable. In the measurement of attenuated fields, battery powered

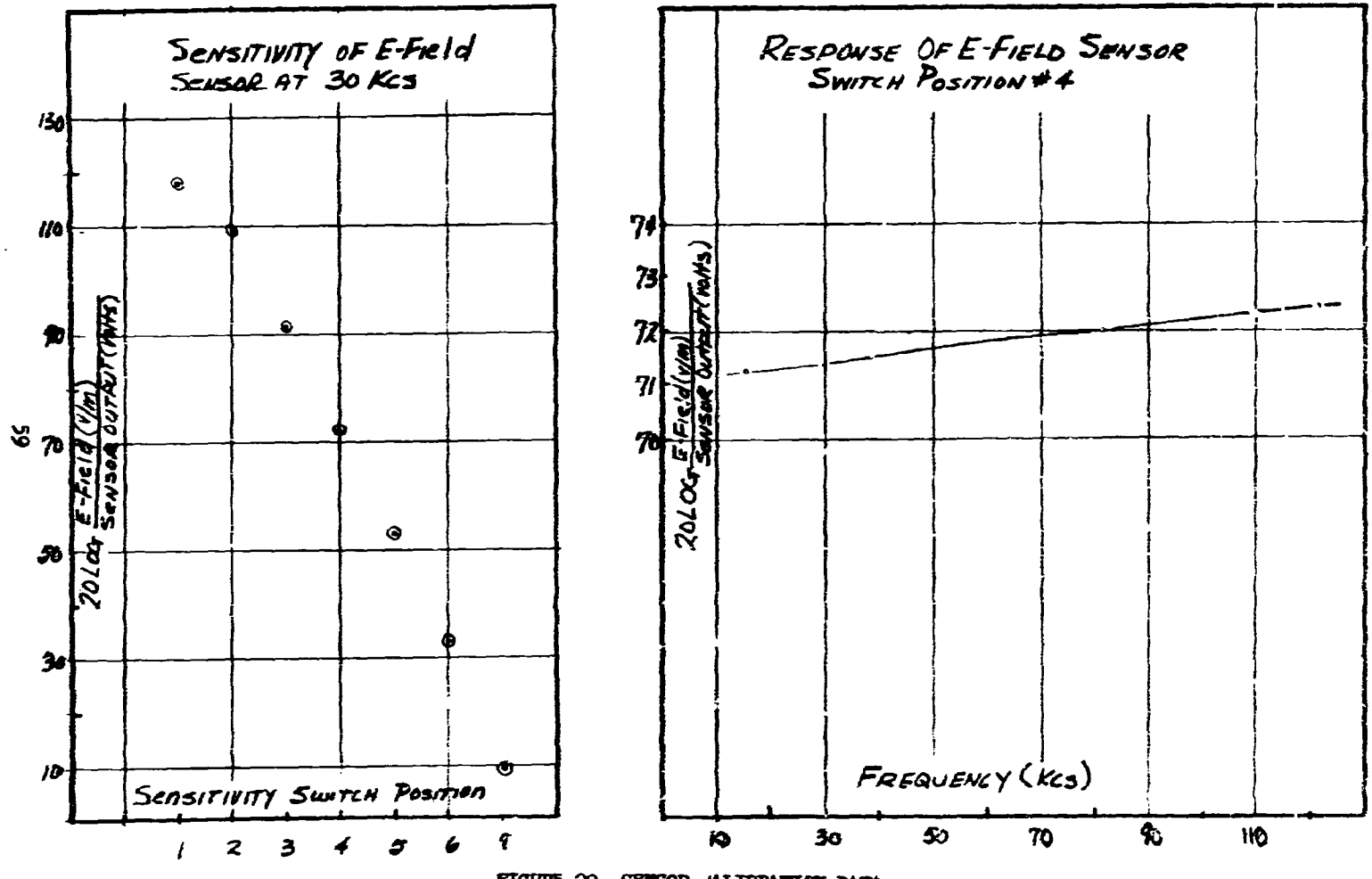

FIGURE 29 SENSOR CALIBRATION DATA

differential amplifiers are utilized within the test environment to boost the signal and preserve the measurement accuracy.

5.4.2 Sensor Description and Response

The loop sensor is a ten turn pickup coil wound on a polyethelyne bobbin precisely fitted within an electrostatic shield. Attempts are made to balance the turns capacitively. Sensor output is a two pin connector for mating with RG-22B/U cable. Series resistance of the sensor is 0.2 ohms and series inductance is 2 microhenries. Response of the sensor is defined by

$$V = k_s \frac{\partial}{\partial t} H \qquad (4)$$

where H is the magnetic field component perpendicular to the plane of the loop

V is the sensor output voltage and

k_s is a constant for the sensor

Steady-state calibration measurements were made on each sensor to determine the value of k_s. Typical data are shown in Figure 30.

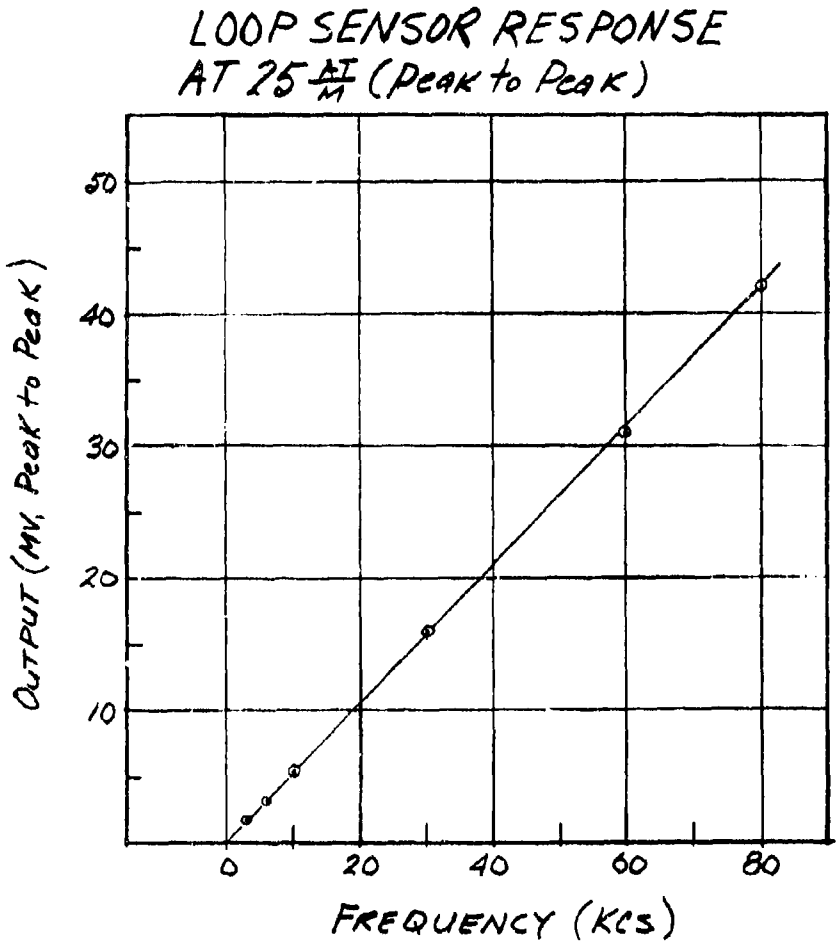

FIGURE 30 LOOP SENSOR RESPONSE

For continuous frequency measurements,

$$V = k_s \omega H \tag{5}$$

The value of k_s from the example is $2.5(10)^{-7}$ volt seconds per gauss.

(U) An operational amplifier is used to directly obtain magnetic field. Operational amplifier response is

$$V_{OUT} = \frac{1}{RC} \int V dt \tag{6}$$

Substituting equation (4) into equation (6) results in

$$V_{OUT} = \frac{k_s}{RC} H \tag{7}$$

From V_{out}, which is available on a scope trace, magnetic field is determined by the application of the constant $\frac{k_s}{RC}$.

An example of the fields generated within the test environment at the EMP Experimental Facility is shown in Figure 31. The fields shown are critically damped and under damped; critical damping is obtained by adding 5.3 ohms to the discharge circuit. The upper trace of both pictures is the sensor output (V_s) directly. The lower traces are the operational amplifier outputs. RC integrator time constant is 10^{-5} in both cases. As shown below the pictures, the peak fields are 104 gauss and 32 gauss, respectively, for the underdamped and the critically damped fields.

SHOT 1-16, 6 OCTOBER 1965

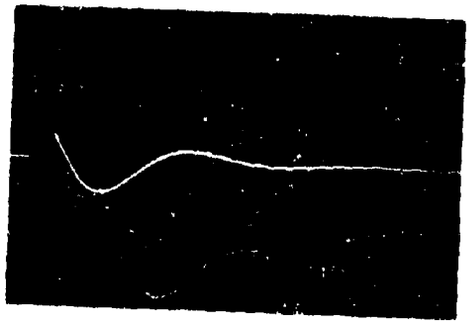

UNDER DAMPING
Damping Resistance 1.8 Ohm
H_o = 104 Gauss

VERTICAL DEFLECTION
Upper Trace: 5.0 Volt/Centimeter
Lower Trace: 1.0 Volt/Centimeter

SHOT 2-9, 6 OCTOBER 1965

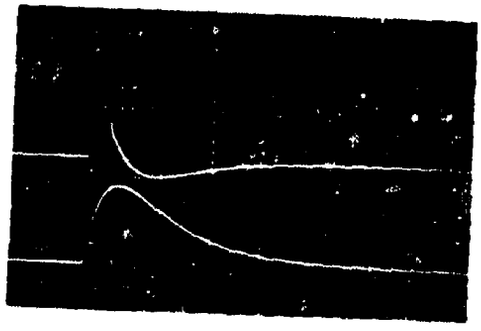

CRITICAL DAMPING
Damping Resistance 7.1 Ohm
H_o = 32 Gauss

VERTICAL DEFLECTION
Upper Trace: 1.0 Volt/Centimeter
Lower Trace: 0.5 Volt/Centimeter

HORIZONTAL SWEEP
10 Microseconds/Centimeter on
Both Traces

UPPER TRACE
$V_1 = k_s \frac{d}{dt} H_o$

LOWER TRACE
$V_2 = \frac{k_s H_o}{RC}$

H_o = External Axial Field
k_s = Sensor Response, $2.5(10)^{-7}$ $\frac{\text{V-Sec}}{\text{Gauss}}$
RC = Integrator Time Constant, 10^{-5} Sec.
Integrator Open - Loop Gain = 2500

$H_o(\text{peak}) = \frac{RCV_2 \text{ (peak)}}{k_s}$

$H_o(\text{peak})$ = 104.0 Gauss

$H_o(\text{peak}) = \frac{RCV_2 \text{ (peak)}}{k_s}$

$H_o(\text{peak})$ = 32.0 Gauss

FIGURE 31 MAGNETIC FIELD ENVIRONMENT

6. SHIELDING EXPERIMENTATION

6.1 Description of Test Configuration

A high amplitude pulsed magnetic field was generated within a right square cylindrical coil 1 meter by 1 meter by 1.2 meters axial length using the facilities of the EMP Experimental Facility described in Chapter 4. Semi-infinite conducting cylindrical shells and closed conducting box type configurations were placed within the cylindrical coil as test specimens and were illuminated with the pulsed magnetic field environment. Magnetic fields were measured within these specimens which were constructed of both copper and steel. Figure 32 is representative of the test configuration and shows a flat rectangular steel box used as the test specimen.

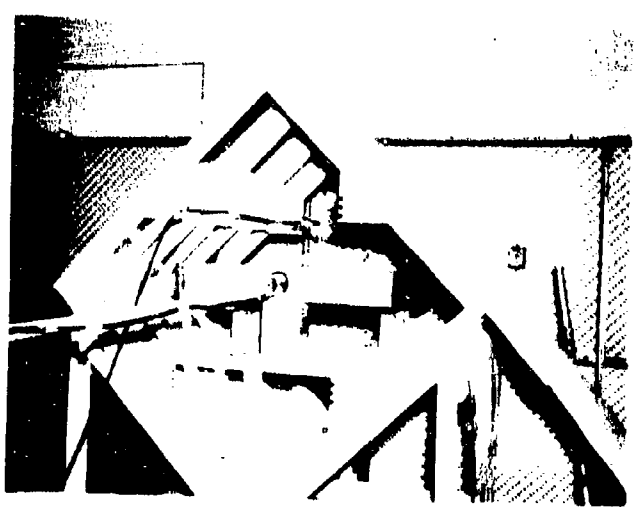

FIGURE 32 TEST CONFIGURATION

Pulsed magnetic fields were monitored using the loop magnetic field sensors described in Section 5.4. Instrumentation cable in all cases was RG22B/U balanced twinax cable terminated in its characteristic impedance at the read-out end. Read-out instrumentation, consisting of camera monitored oscilloscopes and preamplifiers, was located in an adjacent shielded enclosure. All cabling was positioned along magnetic field lines to minimize coupling into the cable twists. In a few cases, balanced differential amplifiers and cable drivers were inserted in the line immediately after the sensors to obtain adequate signal-to-noise ratios.

Within the shielded enclosure, differential amplifiers were used on the front of all oscilloscopes to obtain a 200:1 common mode rejection ratio necessary to minimize electrostatic noise. Tektronix Type G differential preamplifiers were modified for this application. Signals were extracted from the differential preamplifiers and fed into Tektronix Type O operational amplifiers which in some cases were modified for low frequency rejection characteristics.

In all cases, the applied magnetic field was exponentially damped with 30 percent overshoot and with a basic ringing frequency of 30 kilocycles per second as shown in Figure 33.

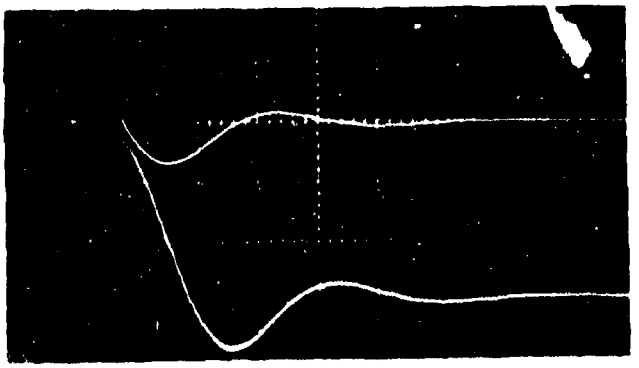

UPPER TRACE
Time Derivative of
Magnetic Field

LOWER TRACE
Magnetic Field

HORIZONTAL SWEEP
10 Microseconds/Centimeter

FIGURE 33 WAVESHAPE OF INCIDENT MAGNETIC FIELD

Low amplitude continuous sine wave attenuation measurements were made for all test configurations in order to support the pulsed experiments. These experiments were conducted at the EMP Experimental Facility and at Procedyne Corporation, New Brunswick, New Jersey.[7] Experiments conducted at USAERDL utilized a 10 centimeter shorted loop with a ferrite current monitor attached. The current generated in the loop located within the test specimen was compared

with the current generated in the same loop located in the incident field. Attenuation insertion techniques were used exclusively to obtain the required dynamic range. All measurements were relative and no attempt was made to establish absolute values.

6.2 Results

6.2.1 Copper Cube Measurements

A 0.33 meter cube of 1.4 mil copper sheet was subjected to incident magnetic fields as described. A loop sensor was placed inside the cube and connected to a shielded twinax cable. The cable passed through a circular waveguide beyond cutoff 3 inches long and 1 inch in diameter, which protruded from the side of the cube. The rate of change of the magnetic field obtained directly from the differential signal on the terminated twinax cable is shown in Figure 34 as the upper trace on Shot Numbers 1-2 and 1-5. The rate of change is a maximum at 7 microseconds, coincident with the peak of the field applied. The peak magnetic field inside the cube can be determined from the lower trace which is the integral related by

$$V_2 = \frac{1}{RC} \int V_1 \, dt \qquad (8)$$

where V_1 is the differential signal obtained from the terminated sensor and RC is the integrator time constant. The magnetic field inside the cube (H) is given by

$$H = \frac{RC}{k_s} V_2 \qquad (9)$$

SHOT 1-2, 1 JUNE 1965 SENSOR AT WAVEGUIDE

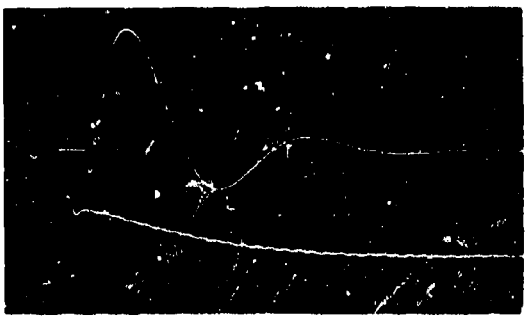

HORIZONTAL SWEEP
UPPER TRACE 10 Microseconds/Centimeter
LOWER TRACE 100 Microseconds/Centimeter
VERTICAL DEFLECTION
0.05 Volts/Centimeter for Both Traces

UPPER TRACE

$$V_1 = k_s \frac{d}{dt} H_1$$

LOWER TRACE

$$V_2 = \frac{k_s}{2RC} H_1$$

$k_s = 2.5(10)^{-7}$ $\frac{\text{Volt-Sec}}{\text{Gauss}}$ Sensor Response Constant

$RC = 10^{-5}$ Integrator Time Constant

H_1 = Axial Field Inside Cube With 100 Gauss Peak External Axial Field

ATTENUATION OF PEAK FIELD

$$20 \text{ Log}_{10} \frac{100}{H_1(\text{peak})} = 20 \text{ Log}_{10} \frac{100}{5.2} = 25.6 \text{ db}$$

INTEGRATOR OPEN LOOP GAIN = 2500 both shots

SHOT 1-5, 1 JUNE 1965 SENSOR AT CENTER OF CUBE

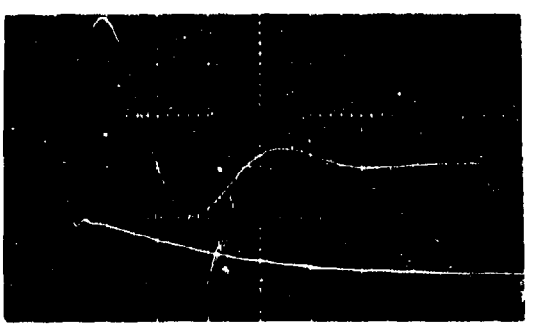

HORIZONTAL SWEEP
UPPER TRACE 10 Microseconds/Centimeter
LOWER TRACE 100 Microseconds/Centimeter
VERTICAL DEFLECTION
0.05 Volt/Centimeter for Both Traces

UPPER TRACE

$$V_1 = k_s \frac{d}{dt} H_1$$

LOWER TRACE

$$V_2 = \frac{k_s}{2RC}$$

$k_s = 2.5(10)^{-7}$ $\frac{\text{Volt-Sec}}{\text{Gauss}}$ Sensor Response Constant

$RC = 10^{-5}$ Integrator Time Constant

H_1 = Axial Field Inside Cube With 100 Gauss Peak External Axial Field

ATTENUATION OF PEAK FIELD

$$20 \text{ Log}_{10} \frac{100}{H_1(\text{peak})} = 20 \text{ Log}_{10} \frac{100}{5.0} = 25 \text{ db}$$

FIGURE 34 AXIAL MAGNETIC FIELD INSIDE COPPER CUBE

where k_s is the loop sensor response constant determined experimentally and defined by the equation

$$V_1 = k_s \omega H \tag{14}$$

A factor of two is necessary to account for integration of only one half of the signal. Peak magnetic field attenuation as shown and irrespective of time of occurrence was 25 db.

To determine the uncertainty in the field measurements, the sensitive axis of the loop sensor was rotated to a position orthogonal to the axial field. Figure 35 shows the null signal obtained.

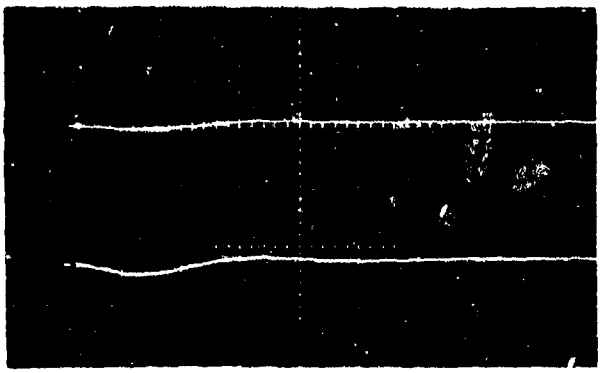

UPPER TRACE
Time Derivative of
Magnetic Field
0.05 Volts/Centimeter
10 Microseconds/Centimeter

LOWER TRACE
Magnetic Field
0.05 Volts/Centimeter
1.0 Microseconds/Centimeter

FIGURE 35 NULL MEASUREMENT, COPPER CUBE

The upper trace with a peak disturbance of 0.01 volts shows that the sensor output may be uncertain in amplitude by as much as 5%. The

lower trace which is the integrator output shows the peak field measured may be uncertain in amplitude by as much as 14%. These measurements probably reflect some error in the positioning of the loop sensor. Low amplitude continuous sine wave attenuation measurements were conducted on the copper cube and are documented in a separate report.[8]

6.2.2 Rectangular Cylinder Measurements

A 0.2 meter by 0.8 meter by 2.4 meter axial length rectangular cylinder was subjected to incident magnetic fields as described. The cylinder was constructed of 1.4 mil copper and the ends were left open. With the exception of a solder joint running axially the length of the cylinder, the surface is continuous. The cylinder was placed coaxially inside the right square cylindrical coil and for all practical purposes appeared semi-infinite.

As in the experiment on the copper cube, loop sensors were used to make field measurements within the cylinder. Cabling and instrumentation were essentially as described in Section 6.2.1. Figure 36 shows a peak internal magnetic field of 5.6 gauss. Attenuation of peak magnetic field is 25 db. The decay rate of the magnetic field is such that half value is obtained at 240 microseconds. Distinct similarities exist between these data and those for the copper cube of comparable cross-section and material.

Null data obtained by rotating the sensor 90 degrees is shown in Figure 37.

SHOT 2-16, 6 OCTOBER 1965

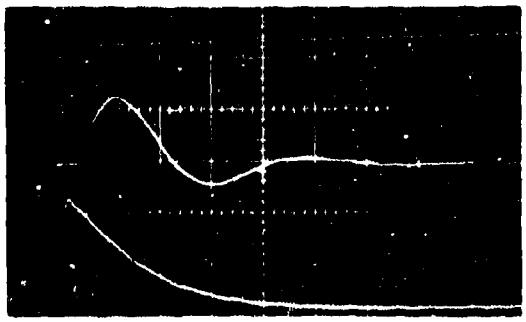

HORIZONTAL SWEEP
  UPPER TRACE 10 Microseconds/Centimeter
  LOWER TRACE 200 Microseconds/Centimeter
VERTICAL DEFLECTION
  UPPER TRACE 0.1 Volts/Centimeter
  LOWER TRACE 0.05 Volts/Centimeter

UPPER TRACE

$$V_1 = k_s \frac{d}{dt} H_i$$

LOWER TRACE

$$V_2 = \frac{k_s}{RC} H_i$$

$k_s = 2.5(10)^{-7}$ $\frac{\text{Volt-Sec}}{\text{Gauss}}$ Sensor Response Constant

$RC = 10^{-5}$ Integrator Time Constant

$$H_i(\text{peak}) = \frac{RC}{k_s} V_2(\text{peak}) = 5.6 \text{ Gauss}$$

H_i = Axial Field Inside Cylinder With 100 Gauss Peak External Axial Field

ATTENUATION OF PEAK FIELD

$$20 \text{ Log}_{10} \frac{100}{H_i(\text{peak})} = 25 \text{ db}$$

INTEGRATOR OPEN LOOP GAIN = 2500 both shots

SHOT 2-18, 6 OCTOBER 1965

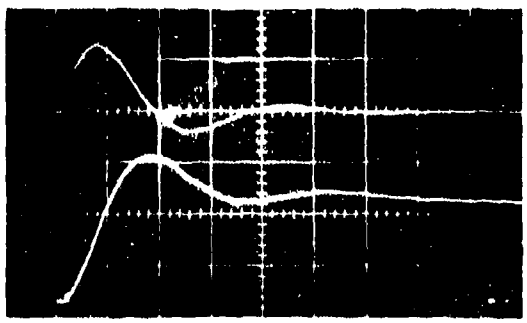

HORIZONTAL SWEEP
  BOTH TRACES 10 Microseconds/Centimeter
VERTICAL DEFLECTION
  UPPER TRACE 0.1 Volts/Centimeter
  LOWER TRACE 0.05 Volts/Centimeter

UPPER TRACE

$$V_1 = k_s \frac{d}{dt} H_i$$

LOWER TRACE

$$V_2 = \frac{k_s}{RC} H_i$$

k_s and RC same as above

$$H_i(\text{peak}) = \frac{RC}{k_s} V_2(\text{peak}) = 5.6 \text{ Gauss}$$

ATTENTUATION OF PEAK FIELD

$$20 \text{ Log}_{10} \frac{100}{H_i(\text{peak})} = 25 \text{ db}$$

FIGURE 36 AXIAL MAGNETIC FIELD
INSIDE RECTANGULAR COPPER CYLINDER

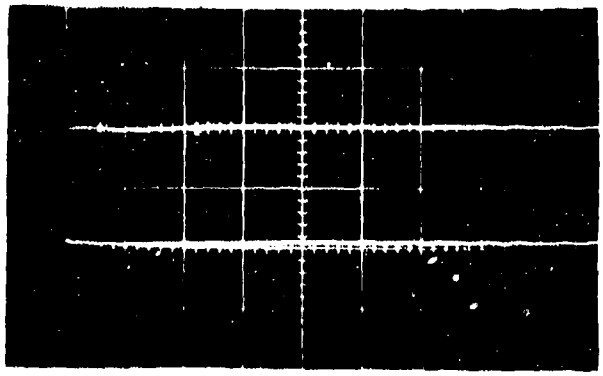

UPPER TRACE
Time Derivative of Magnetic Field
0.1 Volts/Centimeter
10 Microseconds/Centimeter

LOWER TRACE
Magnetic Field
0.05 Volts/Centimeter
200 Microseconds/Centimeter

FIGURE 37 NULL MEASUREMENT ON RECTANGULAR CYLINDER

The disturbances shown are extremely low due to precise positioning of the sensor possible in the open configuration. Maximum uncertainty of the time derivative signal is 5% or less and that for the magnetic field signal is no more than 3%.

Low amplitude continuous sine wave attenuation measurements were made on the rectangular cylinder using the

technique described in Section 6.1. The results at a series of fixed frequencies are tabulated in Figure 38.

FREQUENCY KC	0.5	1	2.5	5	7.5	10	25	50	60	68	75
ATTENUATION db	1.5	4.4	11.0	16.9	20.7	22.7	30.4	36.9	38.2	40	40.3

FIGURE 38 CW ATTENUATION MEASUREMENTS ON A RECTANGULAR CYLINDER

6.2.3 Circular Cylinder Measurements (Copper)

A 0.33 meter diameter by 2.4 meter axial length circular cylinder was subjected to the incident magnetic fields described. The cylinder was constructed of 1.4 mil copper with one axial solder joint running the full length. The cylinder was placed coaxially within the right square cylindrical coil and internal fields were measured as in the experiment on the rectangular cylinder. The results in Figure 39 show typical internal peak magnetic fields of approximately 6 gauss. The decay rate is somewhat faster than that of the rectangular cylinder. The field has collapsed to half value after 190 microseconds.

Typical null data obtained by rotating the sensor 90 degrees are shown in Figure 40.

SHOT 1-3, 8 SEPTEMBER 1965

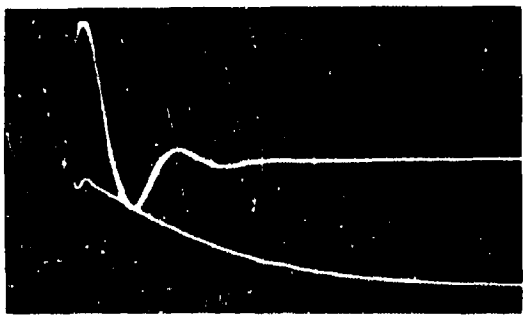

HORIZONTAL SWEEP
UPPER TRACE 20 Microseconds/Centimeter
LOWER TRACE 100 Microseconds/Centimeter
VERTICAL DEFLECTION
BOTH TRACES 0.05 Volts/Centimeter

UPPER TRACE

$$V_1 = k_s \frac{d}{dt} H_i$$

LOWER TRACE

$$V_2 = \frac{k_s}{RC} H_i$$

$k_s = 2.5(10)^{-7}$ Volt-Sec/Gauss Sensor Response Constant

RC = Integrator Time Constant = 10^{-5}

H_i = Axial Field Inside Cylinder With Approximately 100 Gauss Peak External Axial Field

$$H_i(\text{peak}) = \frac{RC}{k_s} V_2 = 6.0 \text{ Gauss}$$

ATTENUATION OF PEAK FIELD

$$-20 \log_{10} H_i(\text{peak}) = -20 \log_{10} \frac{6}{100} = 24.4 \text{ db}$$

INTEGRATOR OPEN LOOP GAIN = 2500 Both Shots

SHOT 1-11, 8 SEPTEMBER 1965

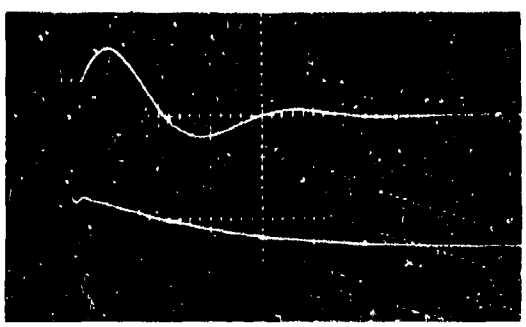

HORIZONTAL SWEEP
UPPER TRACE 10 Microseconds/Centimeter
LOWER TRACE 100 Microseconds/Centimeter
VERTICAL DEFLECTION
BOTH TRACES 0.1 Volts/Centimeter

UPPER TRACE

$$V_1 = k_s \frac{d}{dt} H_i$$

LOWER TRACE

$$V_2 = \frac{k_s}{RC} H_i$$

$RC = 10^{-5}$, $k_s = 2.5(10)^{-7}$

Therefore, $H_i(\text{peak}) = \frac{RC}{k_s} V_2(\text{peak}) =$ 5.8 Gauss

ATTENUATION OF PEAK FIELD

$$-20 \log_{10} \frac{H_i(\text{peak})}{H_o(\text{peak})} = 24.7 \text{ db}$$

FIGURE 39 AXIAL MAGNETIC FIELD INSIDE COPPER CYLINDER

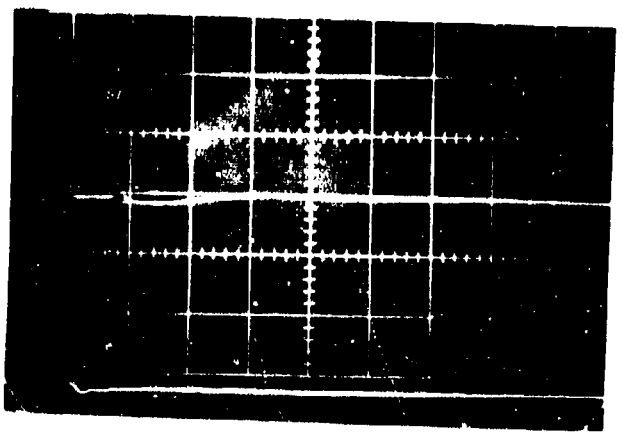

UPPER TRACE
Time Derivative of Magnetic Field
0.05 Volts/Centimeter
10 Microseconds/Centimeter

LOWER TRACE
Magnetic Field
0.02 Volts/Centimeter
100 Microseconds/Centimeter

FIGURE 40 NULL DATA ON COPPER CYLINDER

Maximum uncertainty in the time derivative of magnetic field measurement is 6 percent. Maximum uncertainty in the magnetic field measurement is 3%.

Low amplitude continuous wave attenuation measurements were conducted on the copper cylinder and are documented in a separate report.[9]

6.2.4 Circular Cylinder Measurements (Steel)

In addition to the measurements made on copper

enclosures, measurements were made on steel enclosures in order to relate theoretical work, with a relative permeability of one, to other theoretical work involving relative permeabilities greater than one. A 12 inch diameter by 96 inch axial length steel cylinder was subjected to the described incident magnetic field in the same manner as the copper cylinders. The cylinder was of 1/16 inch 1020 steel with one axial seam welded over the entire length. The results are shown in Figure 41.

As was expected, the attenuation was much greater than that for the copper structures. A peak magnetic field of 0.16 gauss occurs one millisecond after the peak of the applied field. Due to the low signal levels involved with measuring the time derivative of a low frequency field, two independent remote differential amplifiers were used to obtain adequate signal-to-noise ratios. These amplifiers have 64 db of gain and 40 db of gain and are described in Section 5.1.

The uncertainty in the field measurement was determined for the 64 db amplifier instrumentation system. The null data are displayed in Figure 42.

SHOT 1-4, 7 SEPTEMBER 1965

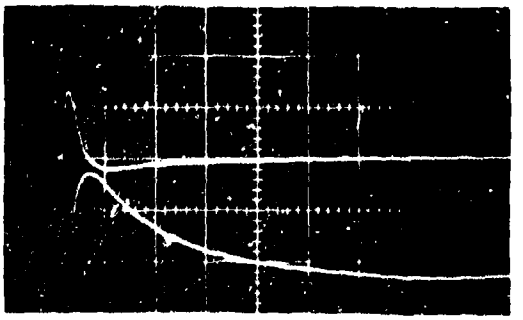

HORIZONTAL SWEEP 2 MILLISECOND/CENTIMETER
VERTICAL DEFLECTION
UPPER TRACE 1.0 Volts/Centimeter
LOWER TRACE 0.5 Volts/Centimeter

UPPER TRACE

$$V_1 = A k_s \frac{d}{dt} H_i$$

LOWER TRACE

$$V_2 = \frac{Ak_s}{RC} H_i, \quad k_s = 75(10)^{-7} \frac{\text{Volt-Sec}}{\text{Gauss}}$$

H_i = Axial Field Inside Cylinder With 67 Gauss External Field
A = Amplifier Gain = 64 db
RC = Integrator Time Constant = $2(10)^{-3}$

$$H_i(\text{peak}) = \frac{RC}{k_s A} V_2(\text{peak}) = 0.16 \text{ Gauss}$$

ATTENUATION OF PEAK FIELD

$$-20 \log_{10} \frac{H_i(\text{peak})}{H_o(\text{peak})} = 52 \text{ db}$$

INTEGRATOR OPEN LOOP GAIN = 2500 Both Shots

SHOT 1-2, 7 SEPTEMBER 1965

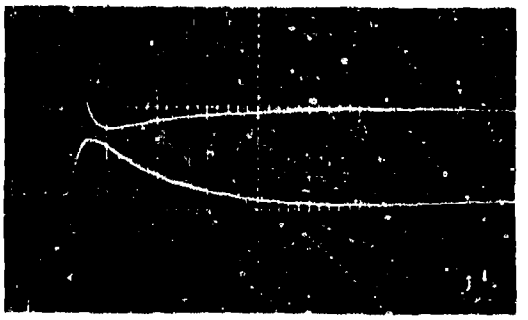

HORIZONTAL SWEEP 2 MILLISECONDS/CENTIMETER
VERTICAL DEFLECTION
UPPER TRACE 0.1 Volts/Centimeter
LOWER TRACE 0.05 Volts/Centimeter

UPPER TRACE

$$V_1 = Ak_s \frac{d}{dt} H_i$$

LOWER TRACE

$$V_2 = \frac{Ak_s}{RC} H_i$$

H_i = Axial Field Inside Cylinder With 67 Gauss (peak) External Field
A = Amplifier Gain = 40 db
RC = Integration Constant = $2(10)^{-3}$
k_s = Sensor Response = $75(10)^{-7} \frac{\text{Volt-Sec}}{\text{Gauss}}$

$$H_i(\text{peak}) = \frac{RC}{k_s A} V_2(\text{peak}) = 0.16 \text{ Gauss}$$

ATTENUATION OF PEAK FIELD

$$-20 \log_{10} \frac{H_i(\text{peak})}{67} = 52 \text{ db}$$

FIGURE 41 AXIAL MAGNETIC FIELD
INSIDE STEEL CYLINDER

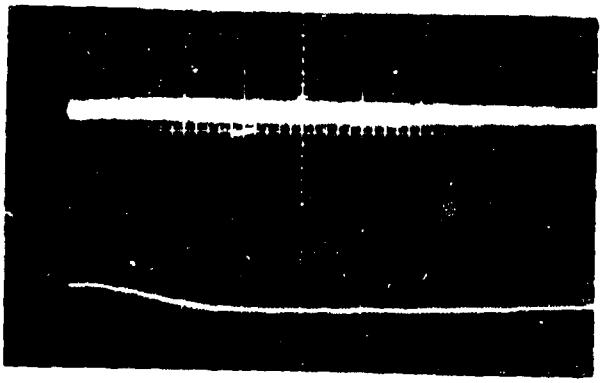

UPPER TRACE
Time Derivative of Magnetic Field
0.2 Volts/Centimeter
500 Microseconds/Centimeter

LOWER TRACE
Magnetic Field
0.2 Volts/Centimeter
500 Microseconds/Centimeter

FIGURE 42 NULL MEASUREMENT ON STEEL CYLINDER

The upper trace shows only amplifier hash during the event; however, the integrated waveform which limits the high frequency signal at 20 db per decade shows a 0.08 volt disturbance or a 14% uncertainty in the data.

Low amplitude continuous sine wave attenuation for the steel cylinder determined as described in Section 6.1 is tabulated in Figure 43. The frequency band over which these measurements were made is less than that of the copper cylinder because of the high attenuations encountered.

FREQUENCY KC	0.5	1	2	3	4	5
ATTENUATION	21.6	30.4	45	55	63.8	72

FIGURE 43 CW ATTENUATION MEASUREMENTS ON A STEEL CYLINDER

6.2.5 Steel Box Measurements

Magnetic field measurements were made on a steel box 3 inches high and 30 inches square for the incident field as described. The box was constructed of 30 gauge steel and had a continuous weld around one of the square sides and along the short dimensioned corners. Figure 44 shows the results of this experiment which was conducted in the same manner as the steel cylinder using two independent remote differential amplifiers. The data are spread from 0.51 gauss to 0.44 gauss peak magnetic field.

The uncertainty in this field measurement is shown by the null data for the 64 db amplifier in Figure 45.

SHOT 1-25, 8 AUGUST 1965

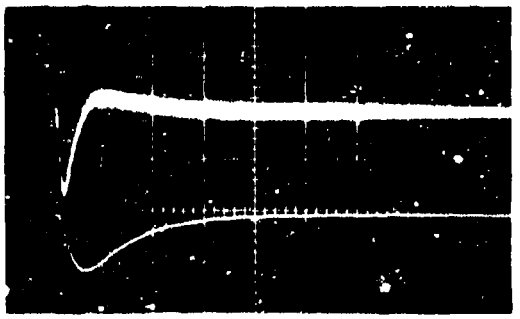

UPPER TRACE

$V_1 = Ak_s \frac{d}{dt} H_1$

LOWER TRACE

$V_2 = \frac{Ak_s}{RC} H_1$

A = 64 db Amplifier Gain

$k_s = 2.5(10)^{-7}$ $\frac{\text{Volt-Sec.}}{\text{Gauss}}$ Sensor Response Constant

RC = $2(10)^{-3}$ Integrator Time Constant

H_1 = Axial Field Inside Steel Box with 100 Gauss (Peak) External Axial Field

$H_1(\text{peak}) = \frac{RC}{k_s A} V_2(\text{peak}) = 0.51$ Gauss

ATTENUATION OF PEAK FIELD

$20 \text{ Log}_{10} \frac{100}{H_1(\text{peak})} = 46.2$ db

INTEGRATOR OPEN LOOP GAIN = 2500 Both Shots

SHOT 1-10, 31 AUGUST 1965

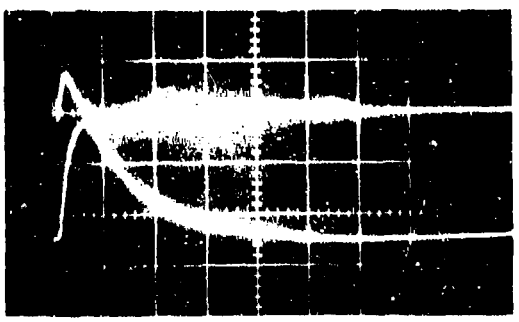

UPPER TRACE

$V_1 = Ak_s \frac{d}{dt} H_1$

LOWER TRACE

$V_2 = A \frac{k_s}{RC} H_1$

A = 40 db

RC = 10^{-4}

$k_s = 2.5(10)^{-7}$ $\frac{\text{Volt-Sec}}{\text{Gauss}}$ Sensor Response Constant

$H_1(\text{peak}) = \frac{RC}{k_s A} V_2(\text{peak}) = 0.44$ Gauss

ATTENUATION OF PEAK FIELD

$20 \text{ Log} \frac{100}{H_1(\text{peak})} = 47.1$ db

HORIZONTAL SWEEP
BOTH TRACES 1 Millisecond/Centimeter
VERTICAL DEFLECTION
BOTH TRACES 0.05 Volts/Centimeter

FIGURE 44 AXIAL MAGNETIC FIELD INSIDE STEEL BOX

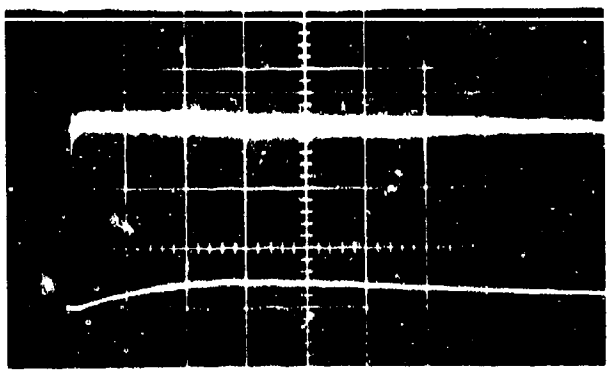

UPPER TRACE
Time Derivative of Magnetic Field
0.5 volts/centimeter
500 microseconds/centimeter

LOWER TRACE
Magnetic Field
0.1 Volts/Centimeter
500 Microseconds/Centimeter

FIGURE 45 NULL DATA FOR STEEL BOX AND 64 db AMPLIFIER

Only the amplifier hash is present in the upper trace. In the lower trace, a 0.04 peak disturbance is present; however, it occurs at a later time than the peak field data. At the time the data are at a peak, only a 20% disturbance is present. Decay rate of the field is more in question however.

No continuous wave attenuation measurements were made on the steel box since the short dimension would not allow placement of the 10 centimeter loop. It would be expected, however, that these measurements would resemble those taken on the steel cylinder discussed in Section 6.2.4.

LIST OF REFERENCES

1. Arthur S. Whitson and Edward F. Vance, Electromagnetic Field Distortions In and Near Buried Cables and Bunkers (U), Air Force Weapons Laboratory Report No. AFWL-TR-65-39, September 1965, Unclassified.

2. Ibid.

3. Ronald J. Bostak, A Nuclear Electromagnetic Pulse Experimental Facility (U), Final Report, DASA Report Number 1563, USAERDL, Fort Belvoir, Va., 15 September 1964, FOR OFFICIAL USE ONLY.

4. Robert Staffin, Final Technical Report (U), Contract DA-44-009-AMC-480(T), Procedyne Corporation for USAERDL, Fort Belvoir, Va., to be published, Unclassified.

5. Seymour Glasser and Hector Nacimento, Electromagnetic Field Sensors (U), Final Technical Report, NRA, Incorporated for USAERDL, Fort Belvoir, Virginia, to be published, Unclassified.

6. G. S. Parks and L. E. Orsak, Electric Field Sensors and Design Assistance for USAERDL Simulation Facility (U), Final Technical Report, Stanford Research Institute for USAERDL, Fort Belvoir, Va., August 1965, Unclassified.

7. Robert Staffin.

8. Ibid.

9. Ibid.

UNCLASSIFIED
Security Classification

DOCUMENT CONTROL DATA - R&D

(Security classification of title, body of abstract and indexing annotation must be entered when the overall report is classified)

1 ORIGINATING ACTIVITY (Corporate author)

U. S. Army Engineer Research and Development Laboratories

2a REPORT SECURITY CLASSIFICATION

UNCLASSIFIED

2b GROUP

3 REPORT TITLE

NUCLEAR ELECTROMAGNETIC PULSE SIMULATION STUDIES IN SUPPORT OF THE NIKE-X ELECTRICAL POWER SYSTEM PROGRAM (REVISED)

4 DESCRIPTIVE NOTES (Type of report and inclusive dates)

Final Technical Report, 1 November 1964 - 31 October 1965

5 AUTHOR(S) (Last name, first name, initial)

Bostak, Ronald J.
Bemis, A. Russell

6 REPORT DATE	7a TOTAL NO OF PAGES	7b NO OF REFS
1 May 1966	98	9

8a CONTRACT OR GRANT NO	9a ORIGINATOR'S REPORT NUMBER(S)
b. PROJECT NO.	
c.	9b OTHER REPORT NO(S) (Any other numbers that may be assigned this report)
d.	

10 AVAILABILITY/LIMITATION NOTICES

All distribution of this report is controlled. Qualified DDC users should request through Office, Chief of Engineers, DA, ATTN: ENGMC-ED, Washington, D. C. 20315.

11 SUPPLEMENTARY NOTES	12 SPONSORING MILITARY ACTIVITY
	Office, Chief of Engineers

13 ABSTRACT

This report presents the results that have been achieved at USAERDL during the period November 1964 through October 1965 in nuclear EMP simulation studies and experimentation in support of the Nike-X electrical power system research and development program. These studies and experiments can be classified as EMP vulnerability testing of existing systems, basic EMP energy coupling experimentation, and EMP simulation or experimental facility design which includes electromagnetic field measurement instrumentation design and development. The experimental results in this report are documented as companion data to theoretical results published in a previous report.

DD FORM 1 JAN 64 1473

UNCLASSIFIED
Security Classification

Security Classification

14. KEY WORDS	LINK A		LINK B		LINK C	
	ROLE	WT	ROLE	WT	ROLE	WT

INSTRUCTIONS

1. ORIGINATING ACTIVITY: Enter the name and address of the contractor, subcontractor, grantee, Department of Defense activity or other organization *(corporate author)* issuing the report.

2a. REPORT SECURITY CLASSIFICATION: Enter the overall security classification of the report. Indicate whether "Restricted Data" is included. Marking is to be in accordance with appropriate security regulations.

2b. GROUP: Automatic downgrading is specified in DoD Directive 5200.10 and Armed Forces Industrial Manual. Enter the group number. Also, when applicable, show that optional markings have been used for Group 3 and Group 4 as authorized.

3. REPORT TITLE: Enter the complete report title in all capital letters. Titles in all cases should be unclassified. If a meaningful title cannot be selected without classification, show title classification in all capitals in parenthesis immediately following the title.

4. DESCRIPTIVE NOTES: If appropriate, enter the type of report, e.g., interim, progress, summary, annual, or final. Give the inclusive dates when a specific reporting period is covered.

5. AUTHOR(S): Enter the name(s) of author(s) as shown on or in the report. Enter last name, first name, middle initial. If military, show rank and branch of service. The name of the principal author is an absolute minimum requirement.

6. REPORT DATE: Enter the date of the report as day, month, year; or month, year. If more than one date appears on the report, use date of publication.

7a. TOTAL NUMBER OF PAGES: The total page count should follow normal pagination procedures, i.e., enter the number of pages containing information.

7b. NUMBER OF REFERENCES: Enter the total number of references cited in the report.

8a. CONTRACT OR GRANT NUMBER: If appropriate, enter the applicable number of the contract or grant under which the report was written.

8b, 8c, & 8d. PROJECT NUMBER: Enter the appropriate military department identification, such as project number, subproject number, system numbers, task number, etc.

9a. ORIGINATOR'S REPORT NUMBER(S): Enter the official report number by which the document will be identified and controlled by the originating activity. This number must be unique to this report.

9b. OTHER REPORT NUMBER(S): If the report has been assigned any other report numbers *(either by the originator or by the sponsor)*, also enter this number(s).

10. AVAILABILITY/LIMITATION NOTICES: Enter any limitations on further dissemination of the report, other than those imposed by security classification, using standard statements such as:

(1) "Qualified requesters may obtain copies of this report from DDC."

(2) "Foreign announcement and dissemination of this report by DDC is not authorized."

(3) "U. S. Government agencies may obtain copies of this report directly from DDC. Other qualified DDC users shall request through _____."

(4) "U. S. military agencies may obtain copies of this report directly from DDC. Other qualified users shall request through _____."

(5) "All distribution of this report is controlled. Qualified DDC users shall request through _____."

If the report has been furnished to the Office of Technical Services, Department of Commerce, for sale to the public, indicate this fact and enter the price, if known.

11. SUPPLEMENTARY NOTES: Use for additional explanatory notes.

12. SPONSORING MILITARY ACTIVITY: Enter the name of the departmental project office or laboratory sponsoring *(paying for)* the research and development. Include address.

13. ABSTRACT: Enter an abstract giving a brief and factual summary of the document indicative of the report, even though it may also appear elsewhere in the body of the technical report. If additional space is required, a continuation sheet shall be attached.

It is highly desirable that the abstract of classified reports be unclassified. Each paragraph of the abstract shall end with an indication of the military security classification of the information in the paragraph, represented as *(TS), (S), (C), or (U)*.

There is no limitation on the length of the abstract. However, the suggested length is from 150 to 225 words.

14. KEY WORDS: Key words are technically meaningful terms or short phrases that characterize a report and may be used as index entries for cataloging the report. Key words must be selected so that no security classification is required. Identifiers, such as equipment model designation, trade name, military project code name, geographic location, may be used as key words but will be followed by an indication of technical context. The assignment of links, rules, and weights is optional.

Security Classification

78,527—Ft Bel